Electronic Supplementary Information

Dope it with germanium: selective access to functionalized Si_5Ge heterocycles

*Benedikt Köstler, Hyunwoo Bae, Jannik Gilmer, Alexander Virovets, Hans-Wolfram Lerner, Philipp Albert, Felipe Fantuzzi, and Matthias Wagner**

Content:

1. Experimental Details and Characterization Data

1.1. General Considerations

All reactions were carried out under an inert-gas atmosphere (dry argon or nitrogen) using standard Schlenk or glove-box techniques. Commercially available starting materials were used as received. *n*-Hexane, C_6H_6, and Et_2O were dried over Na metal; CH_2Cl_2 was dried over CaH_2. All solvents were freshly distilled prior to use. CD_2Cl_2 was stored over molecular sieves (3 Å). NMR spectra were recorded at 298 K on a Bruker Avance III HD 500 spectrometer equipped with a Prodigy BBO 500 S1 probe. $^1H/^{13}C\{^1H\}$ NMR spectra were referenced against (residual) solvent signals (CD_2Cl_2: 5.32 ppm/53.84 ppm).[S1] ^{29}Si NMR spectra were calibrated against external $SiMe_4$ ($\delta(^{29}Si) = 0$). Abbreviations: s = singlet, t = triplet, vsext = virtual sextet, m = multiplet. **Note:** For all Si_5Ge cycles the following numbering scheme is used:

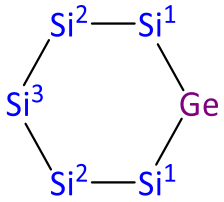

GC-MS (gas chromatography–mass spectrometry) data were recorded using a Shimadzu GCMS-QP2010 SE apparatus. The stationary phase (Restek) had a length of 60 m with an inner diameter of 0.32 mm. The analyte was dissolved in CH_2Cl_2 prior to the measurement. To avoid overloading the MS, a solvent cut was used. Samples were injected at 230 °C and 1/10 thereof was transferred onto the column with a flow rate of 1.86 mL/min, carried by He gas. The oven was heated to 50 °C for 1 min, the temperature was subsequently elevated at a rate of 10 °C/min up to 250 °C and held for 40 min. Finally, the oven temperature was elevated again at a rate of 25 °C/min up to 270 °C and held for 5 min. After a certain retention time τ, the substances exited the column and were ionized with 70 eV, and cationic fragments were measured within a range of m/z = 30–800 (mass per charges). Elemental analysis was performed at the microanalytical laboratory Pascher, Remagen, Germany.

LDI-MS spectra were recorded on a MALDI LTQ Orbitrap XL (Thermo Fisher Scientific) in the negative ion mode. The resolution was set to 60000. The sample spots were prepared inside a glovebox: A solution of the sample in CH_2Cl_2 was transferred to the sample holder by a transfer pipette to form a thin layer of material after evaporation of the solvent. A desiccator was used to maintain the inert-gas atmosphere while bringing the sample holder from the glovebox to the mass spectrometer. The laser energy was set to 50 µJ, and 20 to 30 spectra were

accumulated to increase the signal-to-noise ratio. The isotopic patterns of selected ion species were compared to the theoretical patterns calculated from the elemental composition of the anions using the software mMass.[S2]

1.2. Synthesis of [*n*Bu$_4$N]$_2$[**A**·2Cl]

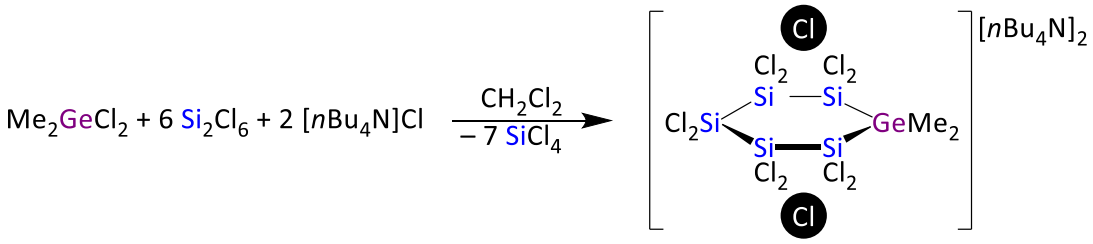

[*n*Bu$_4$N]$_2$[**A**·2Cl]

A solution of [*n*Bu$_4$N]Cl (1.60 g, 5.76 mmol) and Me_2GeCl_2 (0.500 g, 2.88 mmol) in CH_2Cl_2 (15 mL) was prepared in a Schlenk tube. After addition of neat Si_2Cl_6 (4.65 g, 17.3 mmol) at room temperature, the tube was closed and stored for 3 d at room temperature. After all volatiles had been removed under reduced pressure, the colorless sticky residue was washed with *n*-hexane (10 mL) to obtain [*n*Bu$_4$N]$_2$[**A**·2Cl] as a colorless solid. Yield: 3.19 g (2.77 mmol, 96%). Single crystals of [*n*Bu$_4$N]$_2$[**A**·2Cl] suitable for X-ray analysis were grown at room temperature from a solution in CH_2Cl_2, to which 1.5 eq. of *n*-hexane had been added.

^{1}H NMR (500.2 MHz, CD_2Cl_2): δ = 3.21–3.16 (m, 16H; [*n*Bu$_4$N]$^+$), 1.66–1.57 (m, 16H; [*n*Bu$_4$N]$^+$), 1.44 (vsext, ^3J(H,H) = 7.4 Hz, 16H; [*n*Bu$_4$N]$^+$), 0.99 (t, ^3J(H,H) = 7.4 Hz, 24H; [*n*Bu$_4$N]$^+$), 0.53 (s, 3.4H*; $GeMe_2$).

^{13}C{^{1}H} NMR (125.8 MHz, CD_2Cl_2): δ = 59.3 ([*n*Bu$_4$N]$^+$), 24.5 ([*n*Bu$_4$N]$^+$), 20.1 ([*n*Bu$_4$N]$^+$), 13.9 ([*n*Bu$_4$N]$^+$), –0.9 ($GeMe_2$).

^{29}Si{^{1}H} NMR (99.4 MHz, CD_2Cl_2): δ = –6.4 (Si^1), –28.0 (Si^2), –28.6 (Si^3).

LDI-MS(–): *m/z* = 632.54 ([**A**·Cl]$^-$ ≙ ([$C_2H_6Cl_{11}GeSi_5$]$^-$, calcd.: 632.50); Selected further peaks: 562.60 ([$C_2H_6Cl_9GeSi_5$]$^-$, calcd.: 562.57), 534.62 ([$C_2H_6Cl_9GeSi_4$]$^-$, calcd.: 534.59), 430.65 ([Cl_9Si_4]$^-$, calcd.: 430.62), 330.73 ([Cl_7Si_3]$^-$, calcd.: 330.71). All signals show the correct isotope pattern.

Note*: The expected integral value for the proposed structure would be 6H; variations of the pulse delay time had no significant effect. For the following reasons, we nevertheless believe that [*n*Bu$_4$N]$_2$[A**·2Cl] contains a $GeMe_2$ rather than a GeMeCl group: i) In addition to the molecular-ion peak [**A**·Cl]$^-$, the mass spectrum shows several fragments assignable to $GeMe_2$-containing species. We observe no indications for GeMeCl-containing fragments. ii) An X-ray crystallographic analysis gave the best fit to the experimental data with the structural model of [*n*Bu$_4$N]$_2$[**A**·2Cl]. iii) When we performed the synthesis of [*n*Bu$_4$N]$_2$[**A**·2Cl] in a sealed NMR tube (CD_2Cl_2) we observed no ^{1}H NMR signals assignable to $SiMe_nCl_{4-n}$ (n > 0).

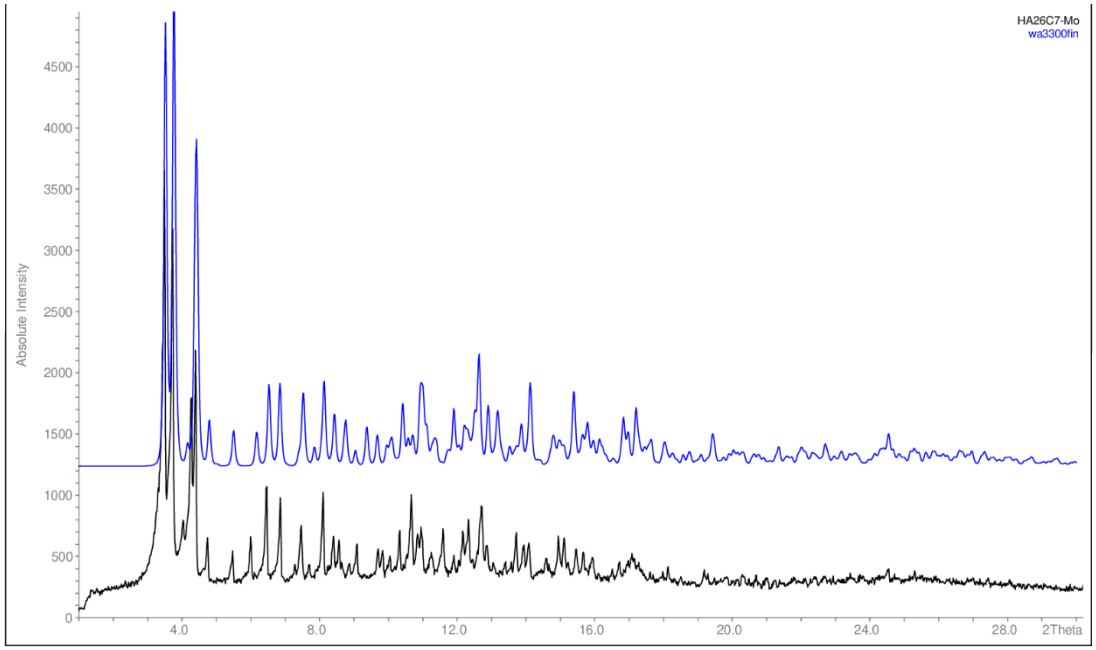

Figure S1. The X-ray powder diffractogram of the bulk product (black; room temperature) shows reasonable agreement with the reference diffractogram simulated from the single-crystal data of $[n\mathrm{Bu_4N}]_2[\mathbf{A}\cdot 2\mathrm{Cl}]$ (blue; –100 °C). Measured at a *STOE-STADI-P* diffractometer.

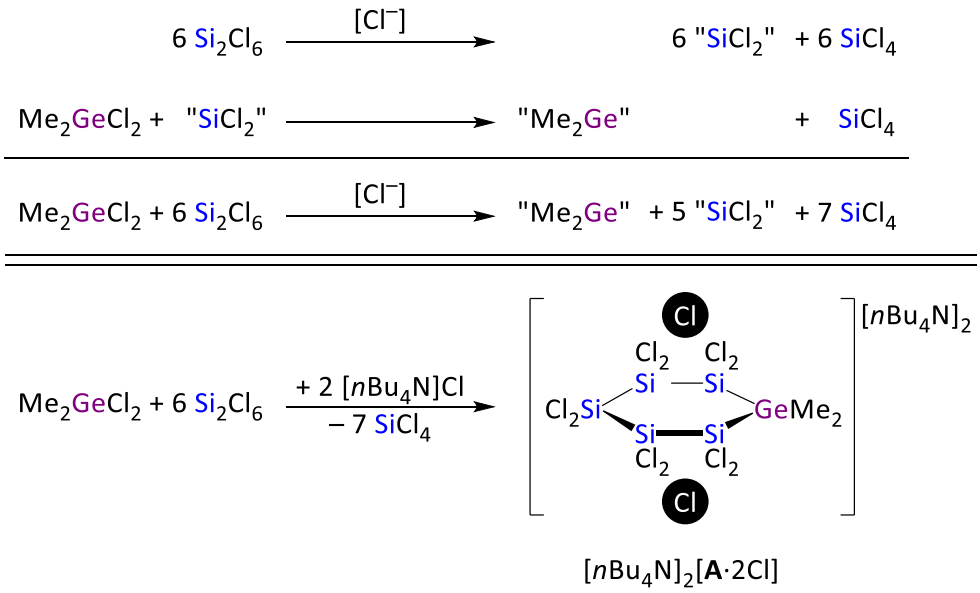

Figure S2. Formalism to rationalize the stoichiometry applied for the synthesis of $[n\mathrm{Bu_4N}]_2[\mathbf{A}\cdot 2\mathrm{Cl}]$.

1.3. Synthesis of A

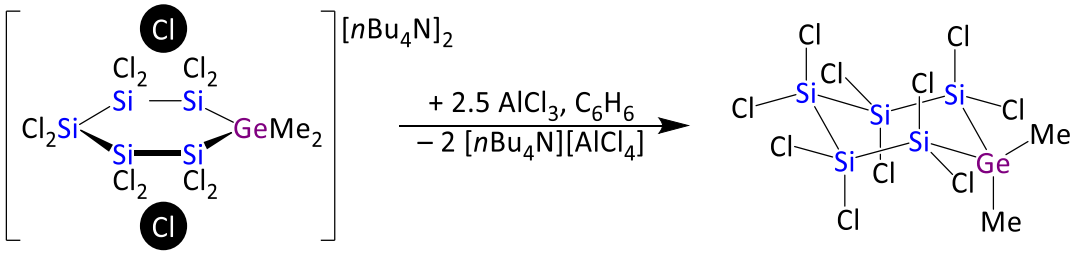

[nBu$_4$N]$_2$[**A**·2Cl]

A Schlenk tube was charged with $AlCl_3$ (0.289 g, 2.17 mmol) and C_6H_6 (20 mL). [nBu$_4$N]$_2$[**A**·2Cl] (1.00 g, 0.867 mmol) was added with stirring at room temperature in four portions at intervals of 30 min. Stirring was continued for 24 h, all volatiles were removed under reduced pressure, and the colorless solid residue was extracted with *n*-hexane (2×10 mL). All volatiles were removed from the extract under reduced pressure to obtain **A** as a colorless solid. Yield: 0.404 g (0.676 mmol, 78%). Single crystals of **A** suitable for X-ray analysis were grown by slow evaporation of a CH_2Cl_2 solution.

Note: The identity of the byproduct [nBu$_4$N][AlCl$_4$] left over from the extraction step was confirmed by ^{27}Al{^{1}H} NMR spectroscopy (δ = 103.8).[S3]

^{1}H NMR (500.2 MHz, CD_2Cl_2): δ = 0.84 (s; $GeMe_2$).

^{13}C{^{1}H} NMR (125.8 MHz, CD_2Cl_2): δ = –5.8 ($GeMe_2$).

^{29}Si{^{1}H} NMR (99.4 MHz, CD_2Cl_2): δ = 15.9 (Si^1), –0.4 (Si^2), –0.6 (Si^3).

1.4. Formation of [*n*Bu$_4$N]$_2$[A·2Cl] through treatment of A with 2 eq. [*n*Bu$_4$N]Cl

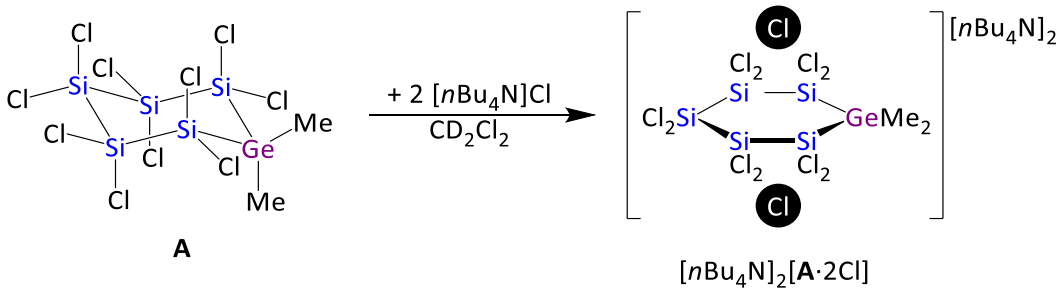

A [*n*Bu$_4$N]$_2$[**A**·2Cl]

A solid mixture of [*n*Bu$_4$N]Cl (0.009 g, 0.03 mmol) and **A** (0.010 g, 0.017 mmol) was prepared in an NMR tube and dissolve in CD_2Cl_2 (0.5 mL). The NMR tube was flame-sealed and stored at room temperature for 1 h. NMR spectroscopy showed a quantitative conversion of **A** to [*n*Bu$_4$N]$_2$[**A**·2Cl] (see Figure S3).

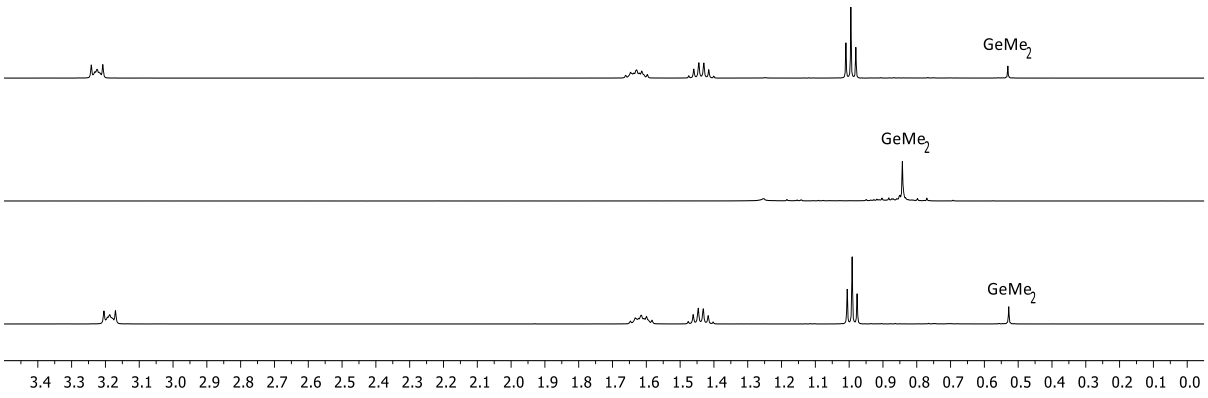

Figure S3. ^{1}H NMR spectrum of the reaction mixture of **A** and 2 eq. [*n*Bu$_4$N]Cl (bottom). Authentic reference spectra of **A** (middle) and [*n*Bu$_4$N]$_2$[**A**·2Cl] (top).

1.5. Synthesis of B

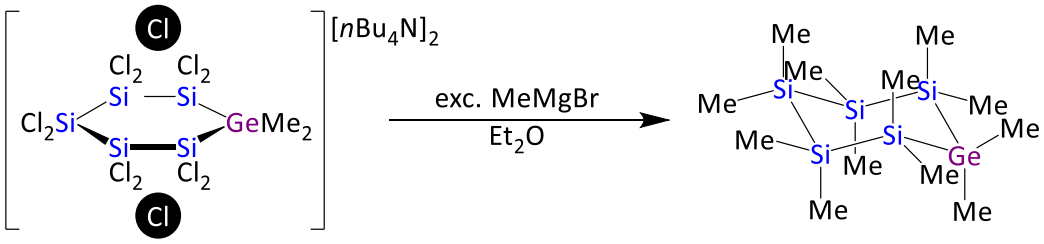

[nBu$_4$N]$_2$[**A**·2Cl]

A suspension of [nBu$_4$N]$_2$[**A**·2Cl] (0.500 g, 0.433 mmol) in Et$_2$O (40 mL) was prepared in a Schlenk tube. MeMgBr (3.0 M in Et$_2$O, 3.0 mL, 9.0 mmol) was added dropwise with stirring via syringe at 0 °C. Stirring was continued at room temperature for 24 h. Neat MeOH (4 mL) was added at 0 °C. All volatiles were removed from the quenched reaction mixture under reduced pressure and the colorless solid residue was extracted with *n*-hexane (2×10 mL). All volatiles were removed from the extract under reduced pressure to obtain **B** as colorless solid. Yield: 0.122 g (0.310 mmol, 72%).

^{1}H NMR (500.2 MHz, CD$_2$Cl$_2$): δ = 0.21 (s, 6H; GeMe$_2$), 0.18 (s, 12H; Si^{1}Me$_2$), 0.14 (s, 12H; Si^{2}Me$_2$), 0.13 (s, 6H; Si^{3}Me$_2$).

^{13}C{^{1}H} NMR (125.8 MHz, CD$_2$Cl$_2$): δ = –5.2 (Si^{1}Me$_2$), –6.0 (Si^{2}Me$_2$ and Si^{3}Me$_2$), –7.0 (GeMe$_2$).

^{29}Si{^{1}H} NMR (99.4 MHz, CD$_2$Cl$_2$): δ = –34.8 (Si^1), –41.6 (Si^2), –42.3 (Si^3).

GC-MS (EI): τ = 20.97 min, m/z = 394 ([M]$^+$), 377 ([M – Me]$^+$), 320 ([M – Me – SiMe$_2$]$^+$), 305 ([M – 2×Me – SiMe$_2$]$^+$). All signals show the correct isotope pattern.

Elemental analysis: Calculated for C$_{12}$H$_{36}$GeSi$_5$ (393.48): C 36.63; H 9.22; Ge 18.5. Found: C 36.91; H 9.22; Ge 19.7.

Note: For comparison, the calculated elemental mass ratios of (SiMe$_2$)$_6$ and (SiMe$_2$)$_4$(GeMe$_2$)$_2$ are C$_{12}$H$_{36}$Si$_6$ (348.93): C 41.31; H 10.40 and C$_{12}$H$_{36}$Ge$_2$Si$_4$ (438.02): C 32.91; H 8.28; Ge 33.2, respectively.

The ^{1}H NMR shift values are in agreement with data reported in the literature.[S4]

1.6. Synthesis of $Cl_3Si–Me_2Ge–SiCl_3$

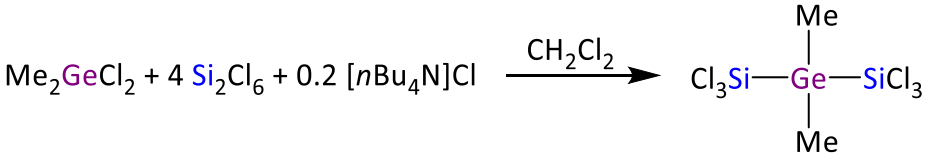

A solution of [*n*Bu$_4$N]Cl (0.320 g, 1.15 mmol) and Me_2GeCl_2 (1.00 g, 5.76 mmol) in CH_2Cl_2 (20 mL) was prepared in a Schlenk flask. Neat Si_2Cl_6 (6.18 g, 23.0 mmol) was added with stirring at room temperature; stirring was continued for 10 min. All volatiles were removed under reduced pressure to obtain a yellow viscous liquid, which was extracted with *n*-hexane (2×10 mL). All volatiles were removed from the extract under reduced pressure to obtain **$Cl_3Si–Me_2Ge–SiCl_3$** as colorless liquid. Yield: 1.47 g (3.94 mmol, 68%).

^{1}H NMR (500.2 MHz, CD_2Cl_2): δ = 0.78 (s; $GeMe_2$).

^{13}C{^{1}H} NMR (125.8 MHz, CD_2Cl_2): δ = –5.2.

^{29}Si{^{1}H} NMR (99.4 MHz, CD_2Cl_2): δ = 13.3.

The ^{13}C and ^{29}Si NMR shift values are in agreement with data reported in the literature.[S5]

1.7. Synthesis of $Cl_3Si–Me_2Ge–Me_2Ge–SiCl_3$

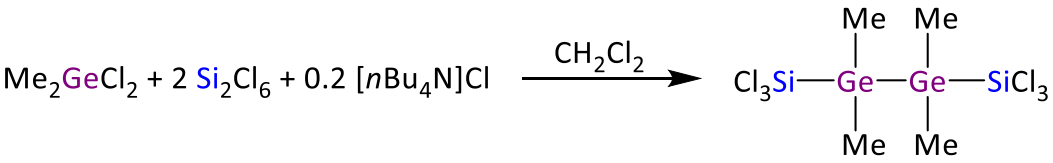

A solution of [*n*Bu$_4$N]Cl (0.160 g, 0.576 mmol) and Me_2GeCl_2 (0.500 g, 2.88 mmol) in CH_2Cl_2 (10 mL) was prepared in a Schlenk flask. Neat Si_2Cl_6 (1.55 g, 5.77 mmol) was added with stirring at room temperature; stirring was continued for 14 d. All volatiles were removed under reduced pressure to obtain a colorless viscous liquid, which was extracted with *n*-hexane (2×5 mL). All volatiles were removed from the extract under reduced pressure to obtain **$Cl_3Si–Me_2Ge–Me_2Ge–SiCl_3$** as colorless liquid. Yield: 0.504 g (1.06 mmol, 74%).

^{1}H NMR (500.2 MHz, CD_2Cl_2): δ = 0.71 (s; $GeMe_2$).

^{13}C{^{1}H} NMR (125.8 MHz, CD_2Cl_2): δ = –4.4.

^{29}Si{^{1}H} NMR (99.4 MHz, CD_2Cl_2): δ = 16.7.

GC-MS (EI): τ = 22.32 min, *m*/*z* = 459 ([M – Me]$^+$), 439 ([M – Cl]$^+$), 339 ([M – $SiCl_3$]$^+$), 267 ([$Me_2Ge–SiCl_3$]$^+$). All signals show the correct isotope pattern.

1.8. Test Reactions: General Considerations

All test reactions compiled in Table S1 were performed in CD_2Cl_2 (0.5 mL) in a flame-sealed NMR tube. The reaction progress was monitored by ^{1}H, $^{13}C\{^{1}H\}$, and $^{29}Si\{^{1}H\}$ NMR spectroscopy. All (NMR detectable) major products were identified.

Note: The heteroadamantanes **4**, **5**, and **6** have already been described by our group.[S6] **4** can be transformed into **5** by treatment with [*n*Bu$_4$N]Cl at room temperature, which explains the formation of **5** in our test experiments (entry 2 and 5). Heating a sample of **5** to 60 °C in the presence of [*n*Bu$_4$N]Cl leads to formation of **6**, which is in line with the result of entry 3.

Background of entry 4: In a second conceivable scenario regarding the assembly mechanism of [*n*Bu$_4$N]$_2$[**A**·2Cl], Si_2Cl_6 remaining after the formation of $Cl_3Si–Me_2Ge–SiCl_3$ could undergo the well-known $Cl^–$-induced conversion to $[(SiCl_2)_6{\cdot}2Cl]^–$,[S7] which then reacts with $Cl_3Si–Me_2Ge–SiCl_3$ to give $[\mathbf{A}{\cdot}2Cl]^–$. However, this alternative pathway can be ruled out since we found that a 1:1-mixture of $[(SiCl_2)_6{\cdot}2Cl]^–$ and $Cl_3Si–Me_2Ge–SiCl_3$ remains unchanged for 3 d.

Table S1. Test reactions concerning the interrelation between selected Me_2Ge-containing oligotetrelanes (entries 1–6). Comparison of the chloride-ion affinities of $(SiCl_2)_6$ and **A** (entries 7 and 8). All reactions were performed in CD_2Cl_2 in sealed NMR tubes.

entry	reactant 1	reactant(s) 2	reaction conditions	reactant 1 consumed?	major product(s)
1	$Cl_3Si–Me_2Ge–SiCl_3$ ≙ **1** (R = Me)	Si_2Cl_6 (4 eq.) [*n*Bu$_4$N]Cl (2 eq.)	7 d, rt	yes	[*n*Bu$_4$N]$_2$[**A**·2Cl] $SiCl_4$
2	$Cl_3Si–Me_2Ge–SiCl_3$ ≙ **1** (R = Me)	[*n*Bu$_4$N]Cl (0.1 eq.)	14 d, rt	partially	**5** **2** (R = Me)
3	$Cl_3Si–Me_2Ge–SiCl_3$ ≙ **1** (R = Me)	[*n*Bu$_4$N]Cl (0.1 eq.)	4 d, 60 °C	yes	**6** **2** (R = Me)
4	$Cl_3Si–Me_2Ge–SiCl_3$ ≙ **1** (R = Me)	[*n*Bu$_4$N]$_2$[$(SiCl_2)_6$·2Cl] (1 eq.)	3 d, rt	no	no reaction
5	**A**	[*n*Bu$_4$N]$_2$[**A**·2Cl] (1 eq.)	1 d, rt	yes	**5** [*n*Bu$_4$N]$_2$[**A**·2Cl], $SiCl_4$ [*n*Bu$_4$N]$_2$[$(SiCl_2)_6$·2Cl]
6	**A**	[*n*Bu$_4$N]Cl (0.1 eq.)	30 d, rt	yes	**1** (R = Me)
7	**A**	[*n*Bu$_4$N]$_2$[$(SiCl_2)_6$·2Cl] (1 eq.)	1 d, rt	yes	[*n*Bu$_4$N]$_2$[$(SiCl_2)_6$·2Cl] **1**, **2** (R = Me), **5**
8	[*n*Bu$_4$N]$_2$[**A**·2Cl]	$(SiCl_2)_6$ (1 eq.)	1 d, rt	yes	[*n*Bu$_4$N]$_2$[$(SiCl_2)_6$·2Cl] **1**, **2** (R = Me), **5**

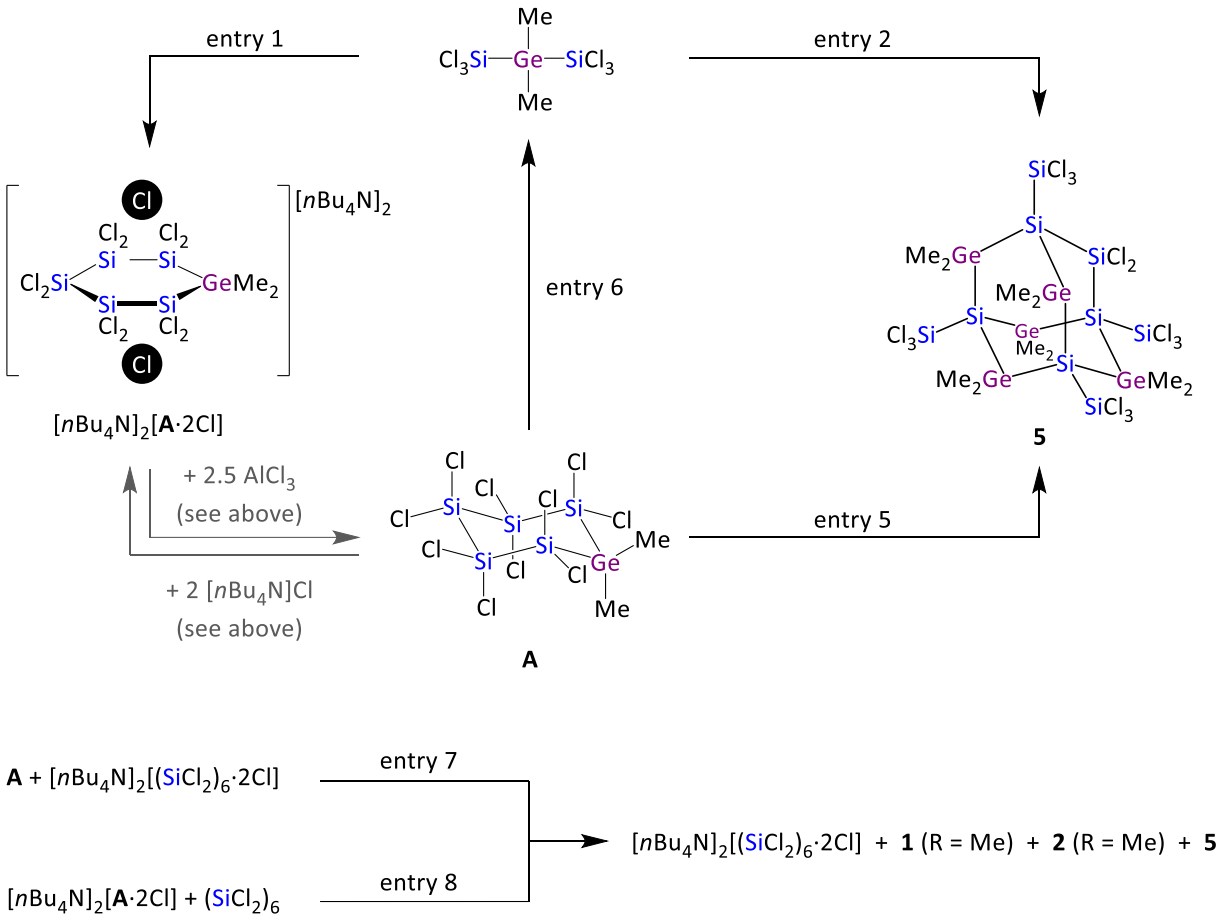

Figure S4. Equations underlying the reactions compiled in Table S1.

2. Plots of ^{1}H, $^{13}C\{^{1}H\}$, $^{29}Si\{^{1}H\}$, and $^{29}Si/^{1}H$ HMBC NMR Spectra

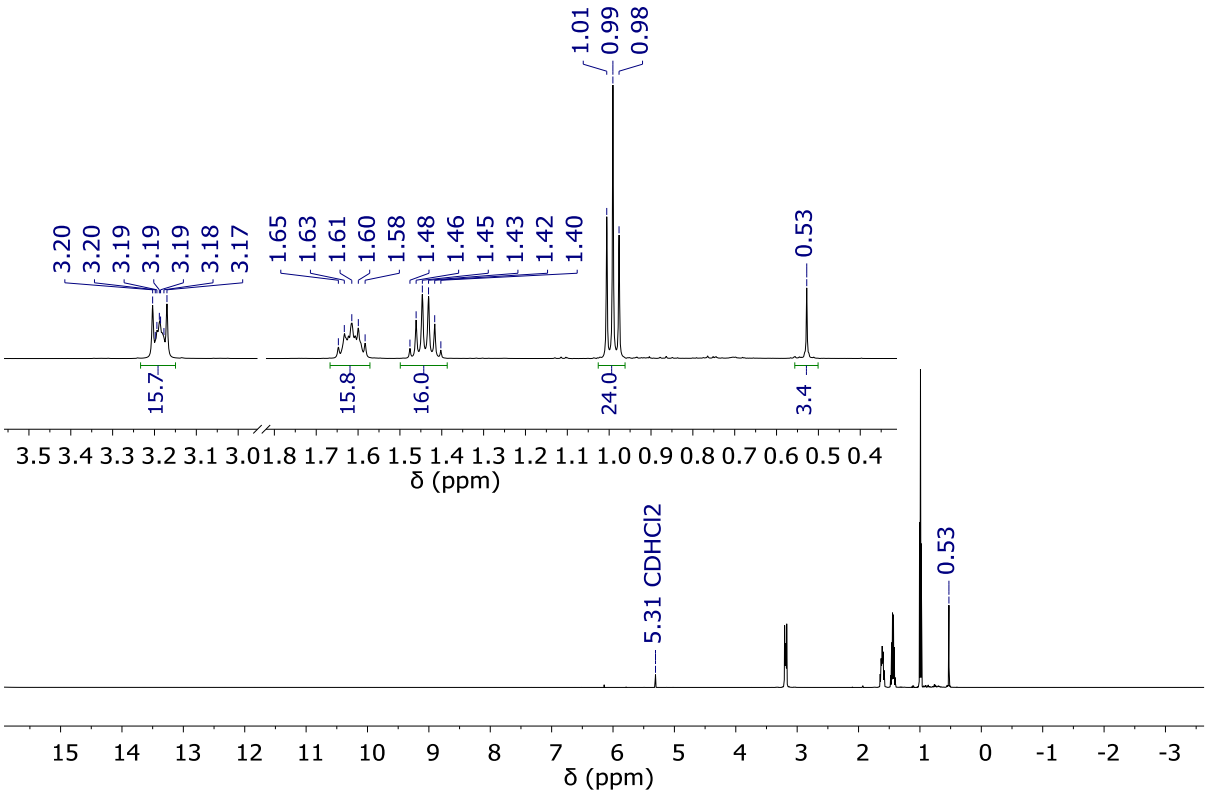

Figure S5. ^{1}H NMR spectrum of $[n\text{Bu}_4\text{N}]_2[\mathbf{A}\cdot 2\text{Cl}]$ (CD_2Cl_2, 500.2 MHz).

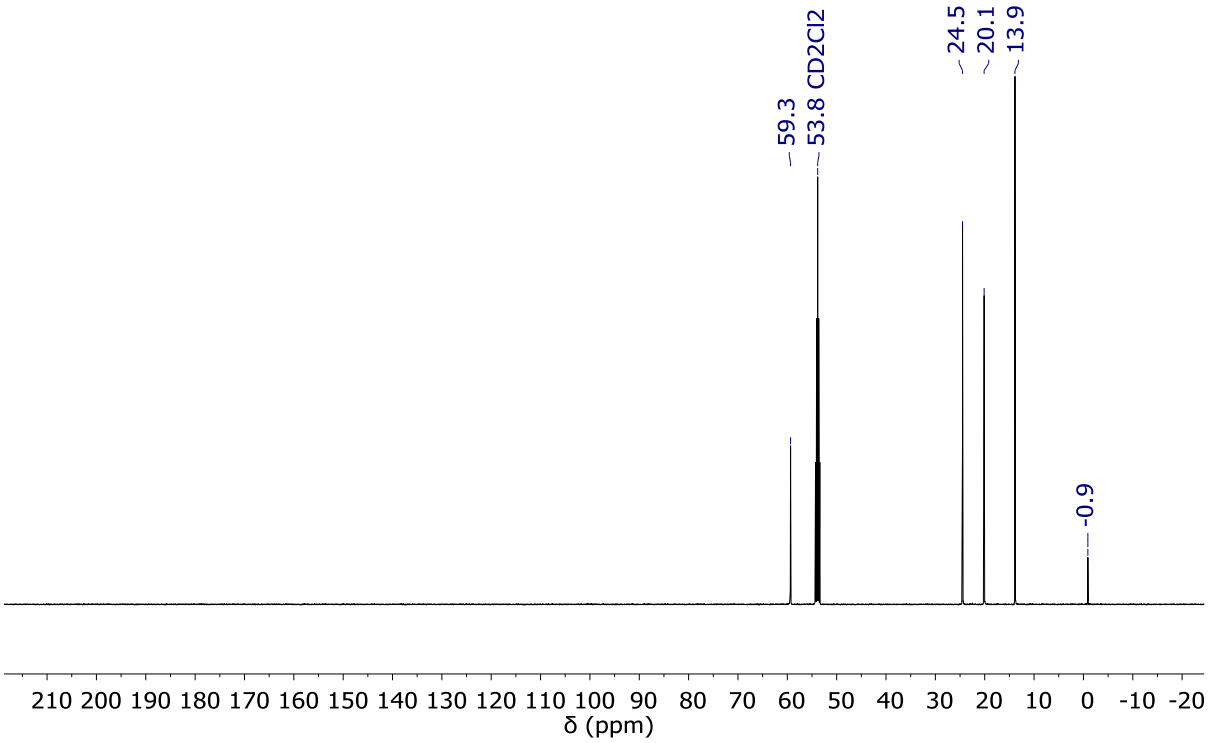

Figure S6. $^{13}C\{^{1}H\}$ NMR spectrum of $[n\text{Bu}_4\text{N}]_2[\mathbf{A}\cdot 2\text{Cl}]$ (CD_2Cl_2, 125.8 MHz).

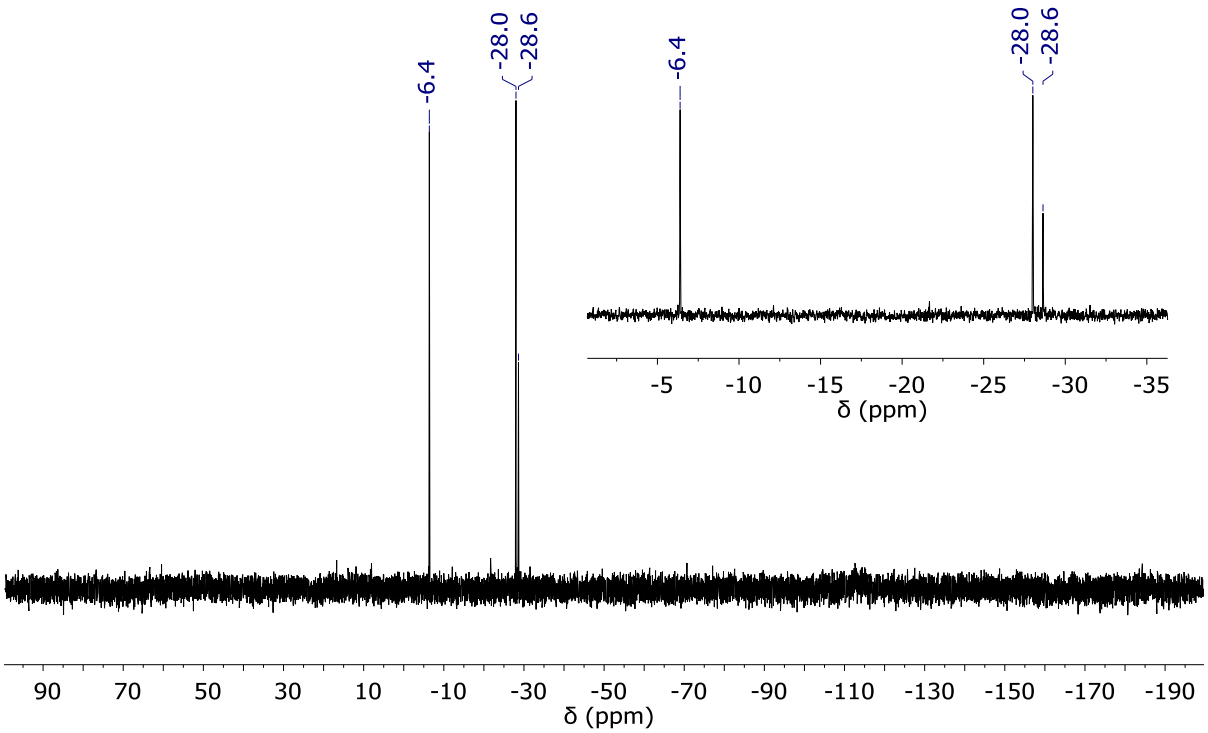

Figure S7. $^{29}Si\{^{1}H\}$ NMR spectrum of $[n\text{Bu}_4\text{N}]_2[\mathbf{A}\cdot 2\text{Cl}]$ (CD_2Cl_2, 99.4 MHz).

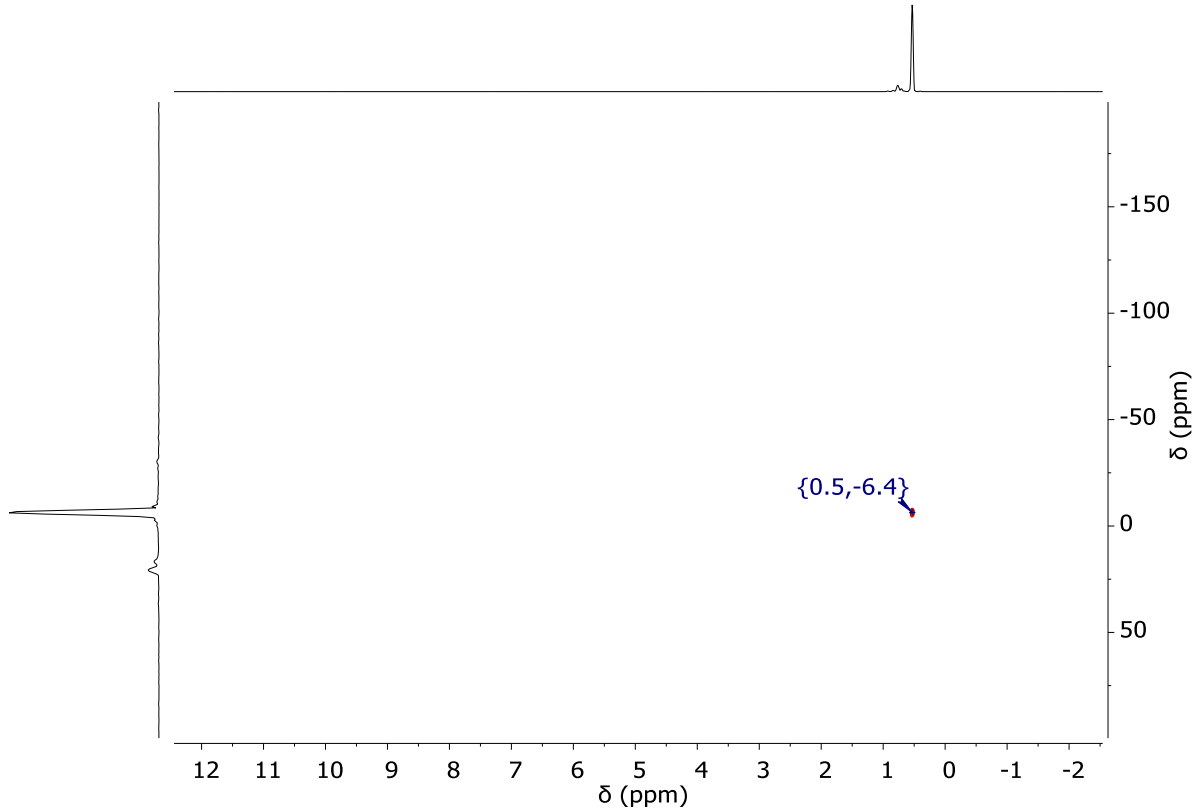

Figure S8. $^{29}Si/^{1}H$ HMBC NMR spectrum of $[n\text{Bu}_4\text{N}]_2[\mathbf{A}\cdot 2\text{Cl}]$.

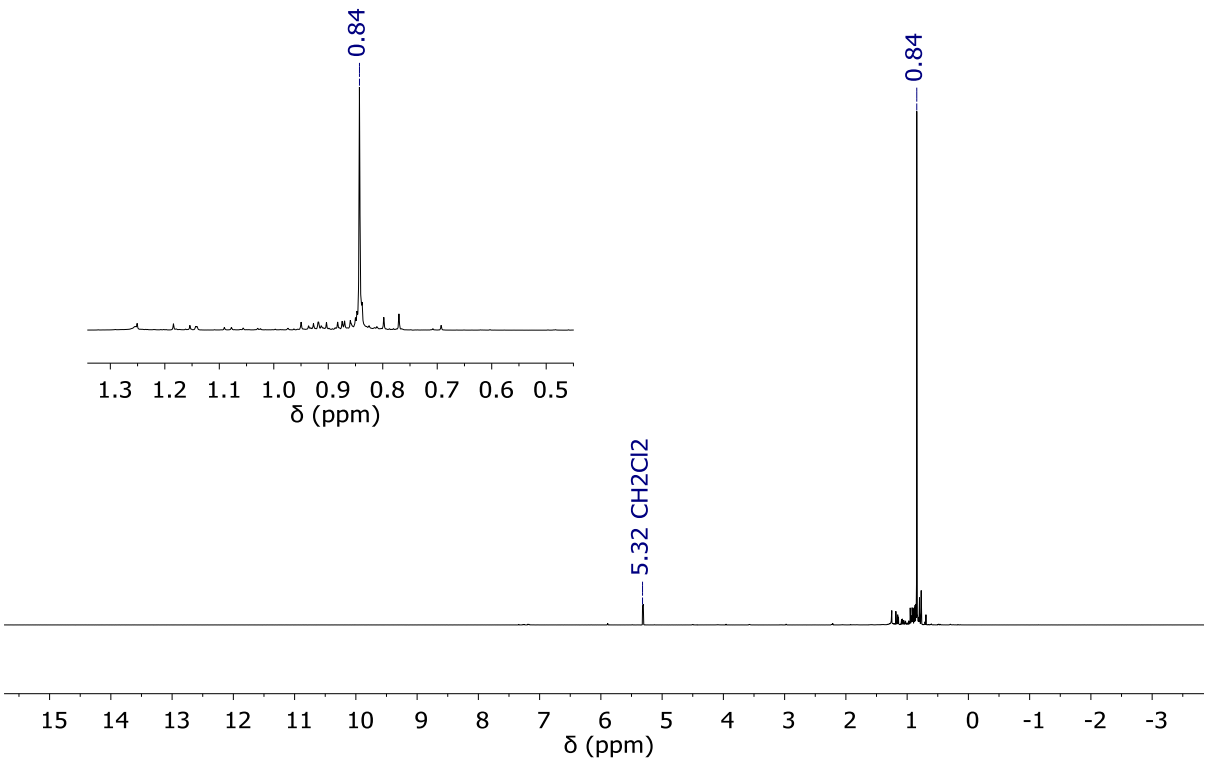

Figure S9. ^{1}H NMR spectrum of **A** (CD_2Cl_2, 500.2 MHz).

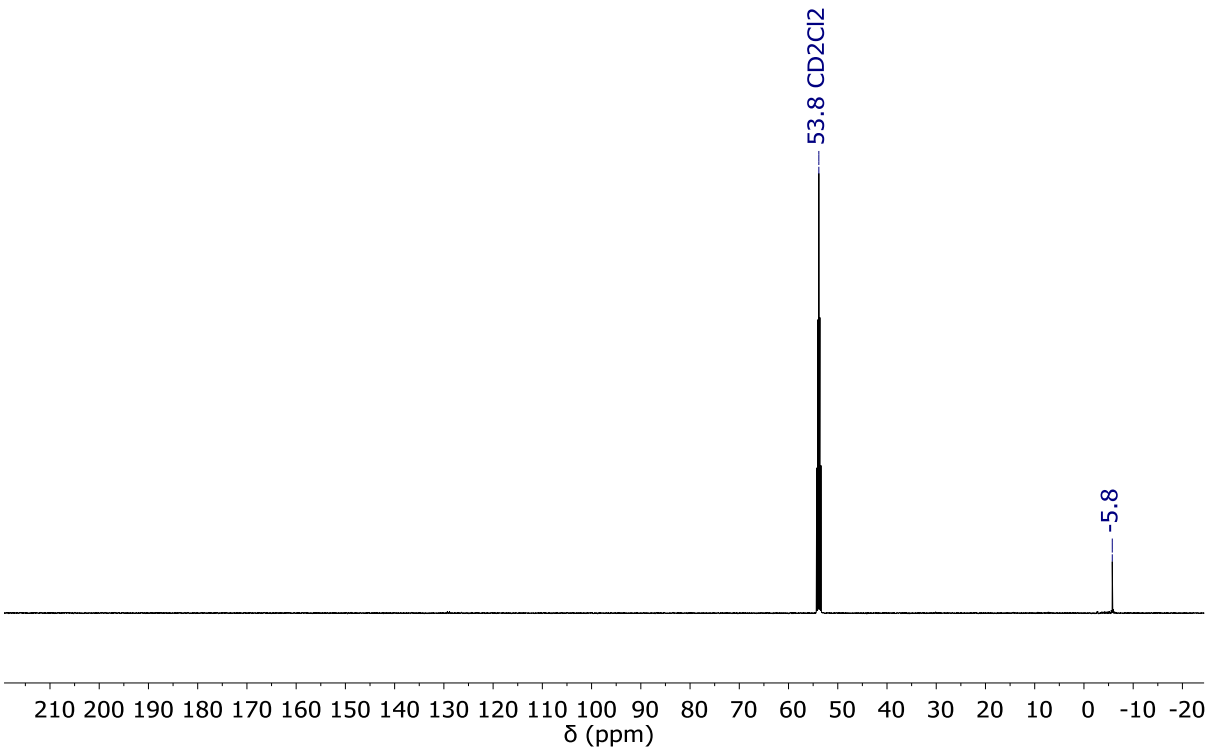

Figure S10. $^{13}C\{^{1}H\}$ NMR spectrum of **A** (CD_2Cl_2, 125.8 MHz).

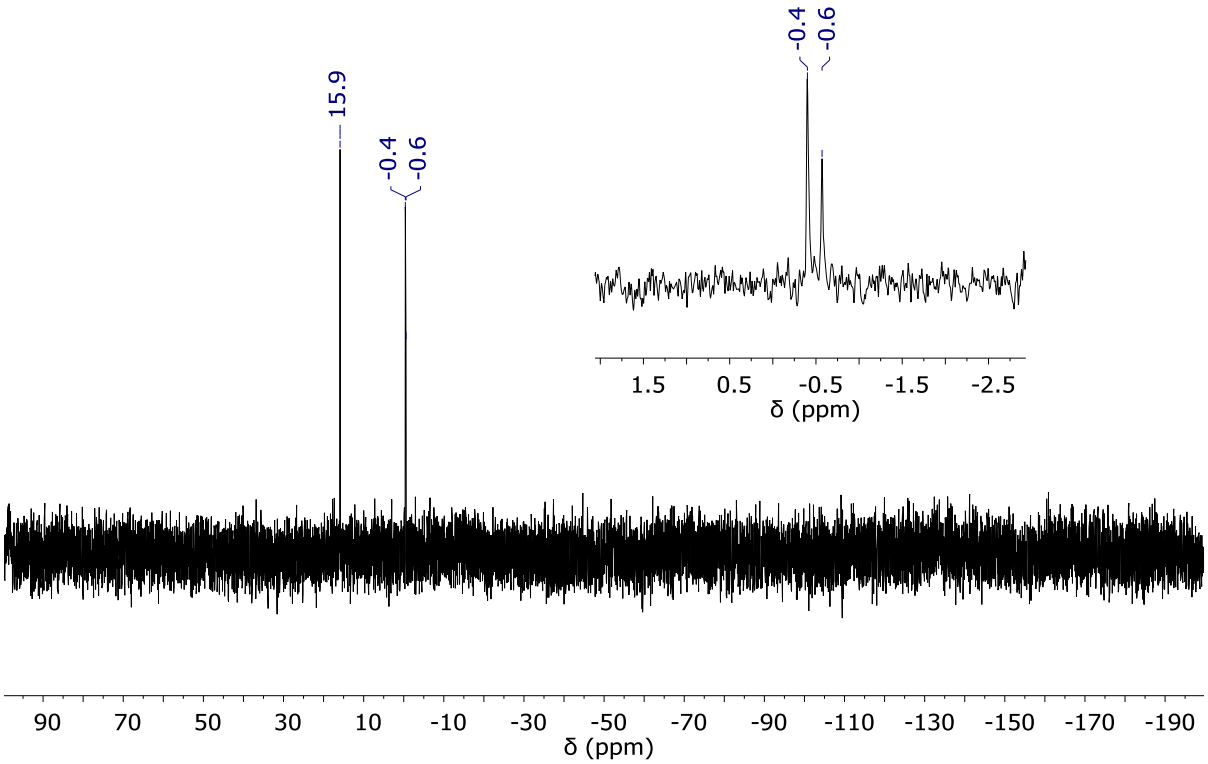

Figure S11. $^{29}Si\{^{1}H\}$ NMR spectrum of **A** (CD_2Cl_2, 99.4 MHz).

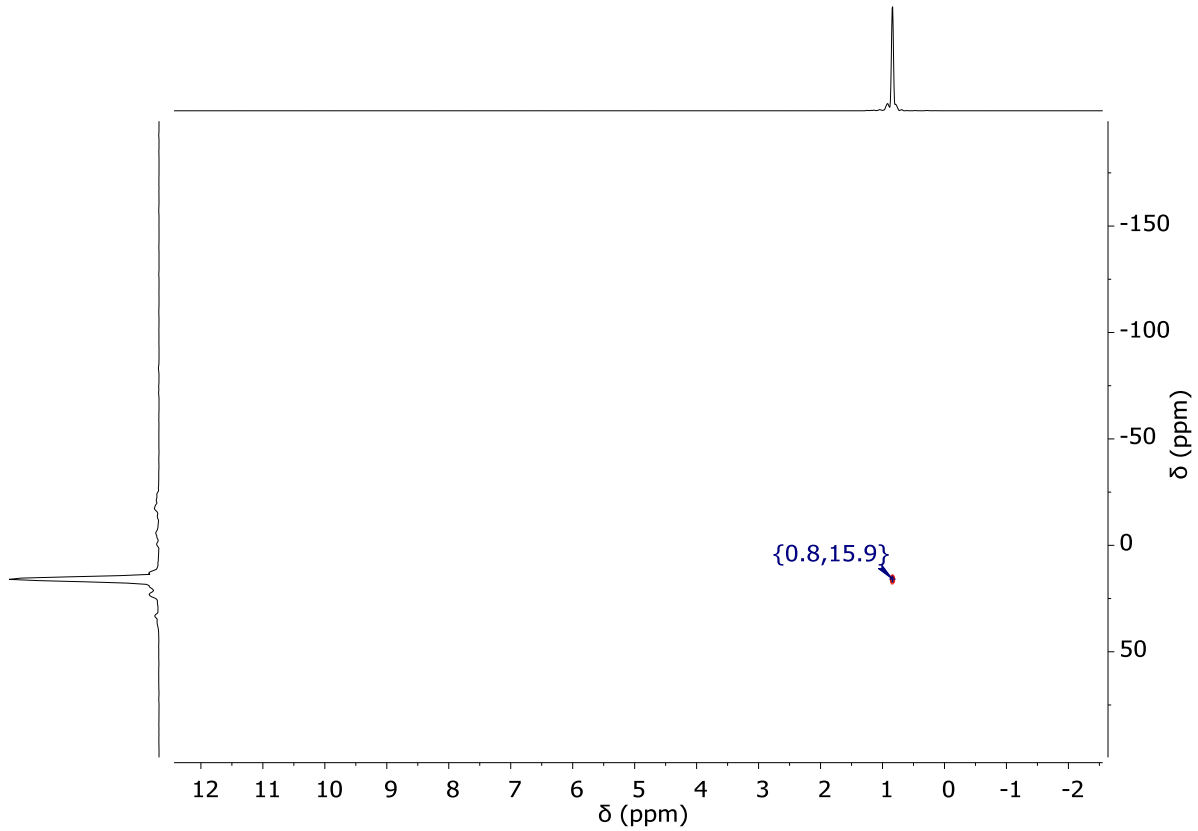

Figure S12. $^{29}Si/^{1}H$ HMBC NMR spectrum of **A**.

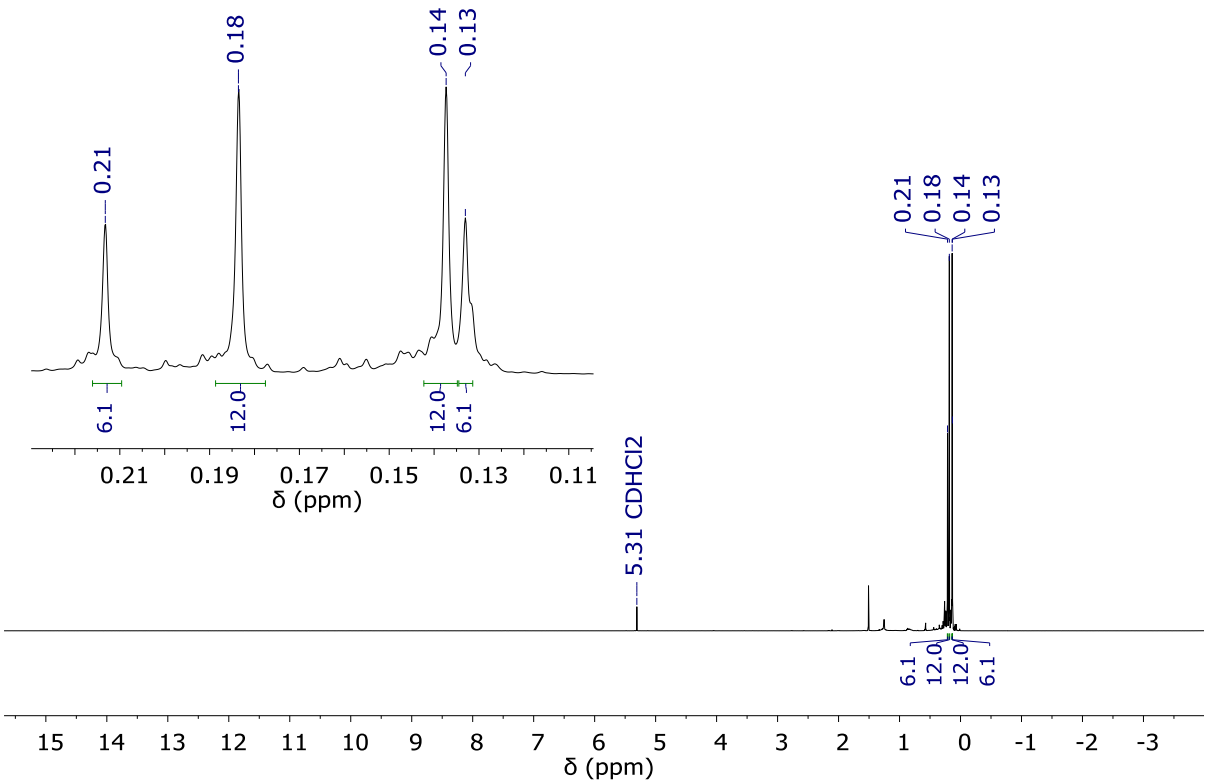

Figure S13. ^{1}H NMR spectrum of **B** (CD_2Cl_2, 500.2 MHz).

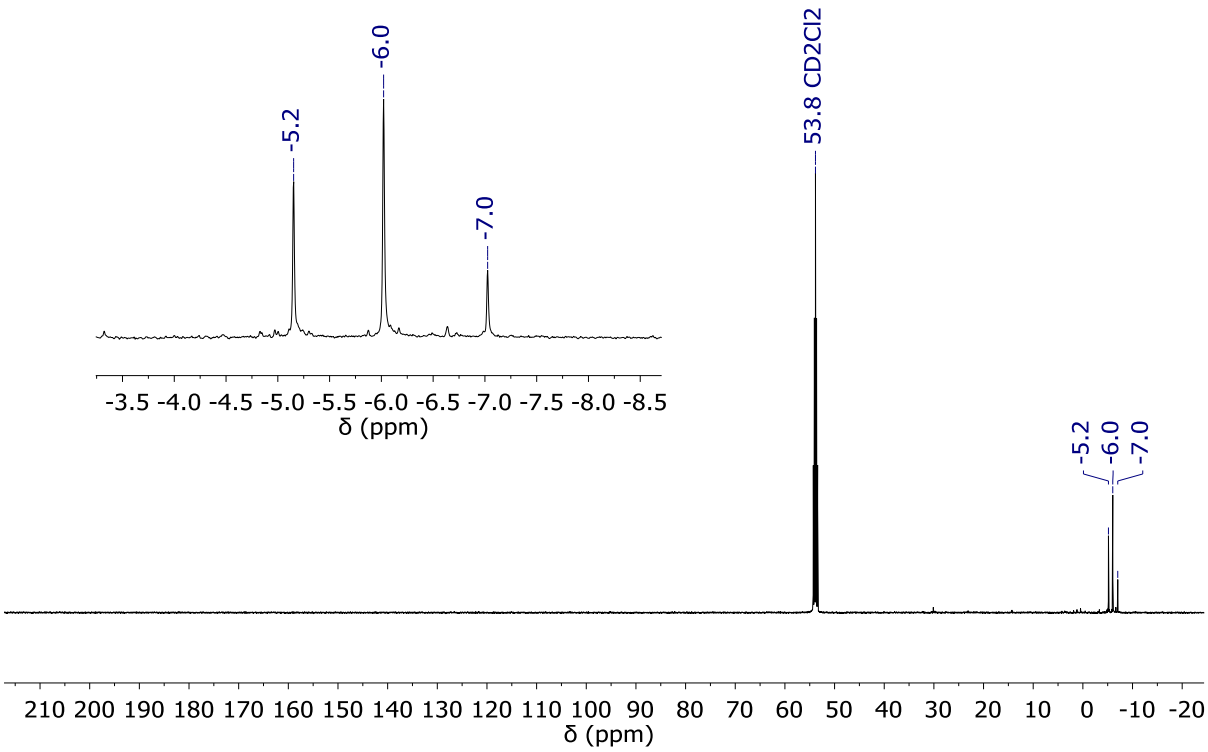

Figure S14. ^{13}C{^{1}H} NMR spectrum of **B** (CD_2Cl_2, 125.8 MHz).

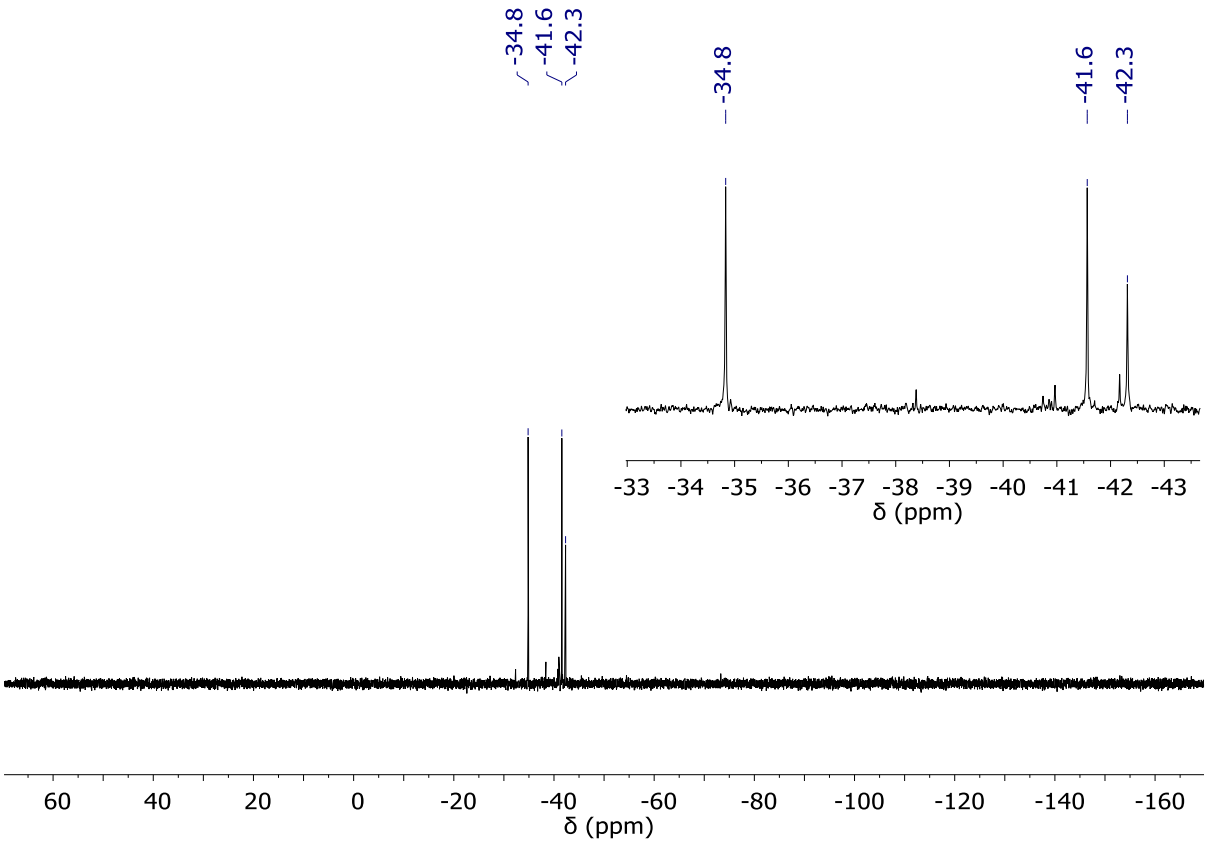

Figure S15. $^{29}Si\{^{1}H\}$ NMR spectrum of **B** (CD_2Cl_2, 99.4 MHz).

Figure S16. $^{29}Si/^{1}H$ HMBC NMR spectrum of **B**.

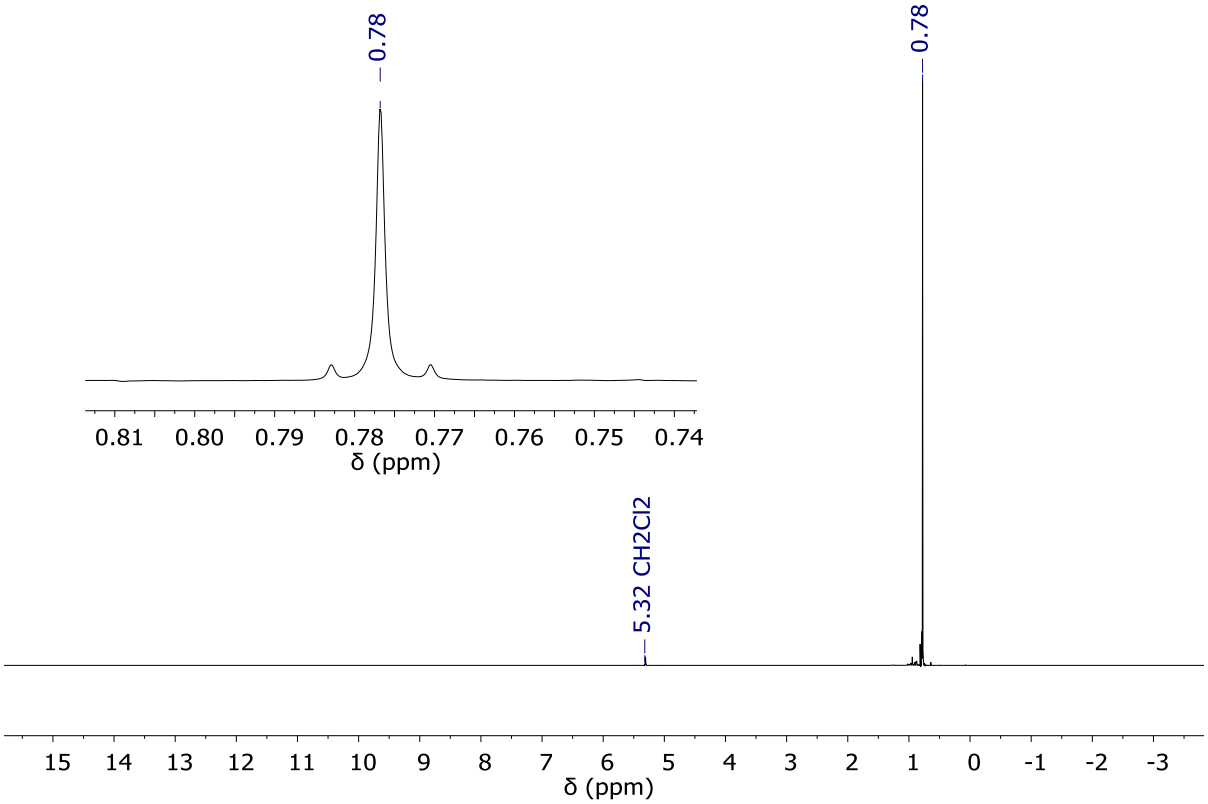

Figure S17. ^{1}H NMR spectrum of $Cl_3Si–Me_2Ge–SiCl_3$ (CD_2Cl_2, 500.2 MHz).

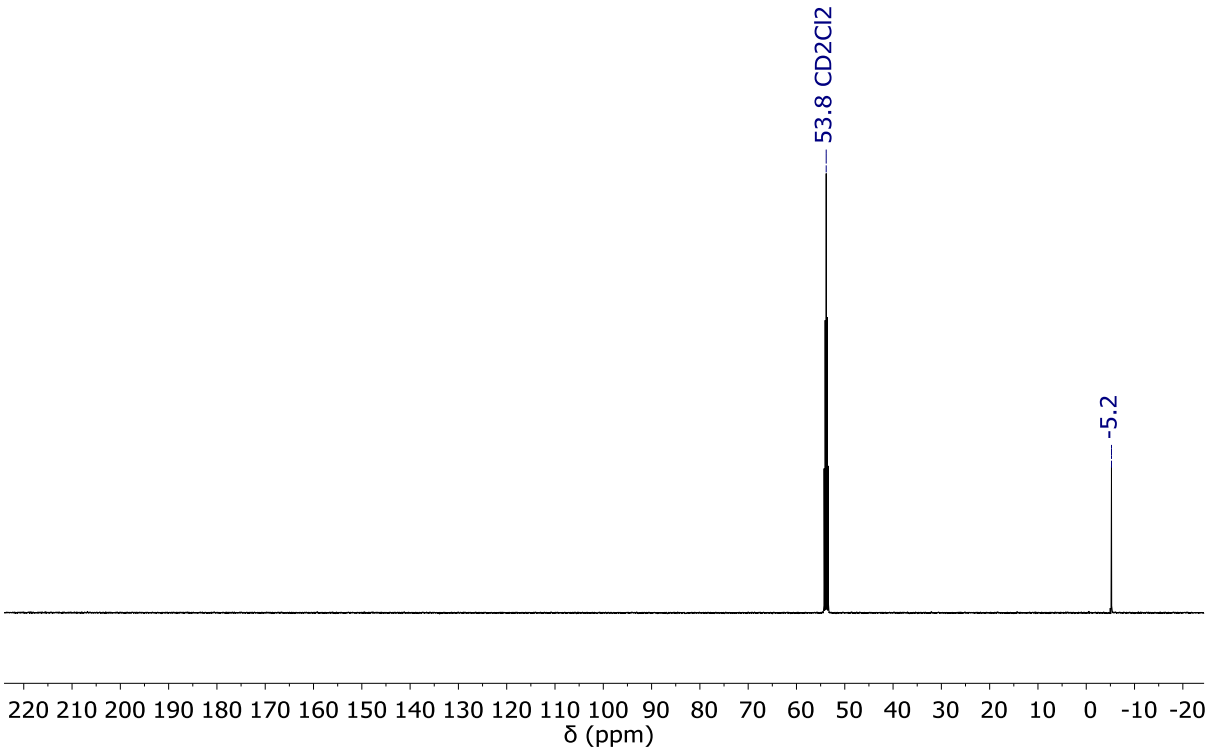

Figure S18. $^{13}C\{^{1}H\}$ NMR spectrum of $Cl_3Si–Me_2Ge–SiCl_3$ (CD_2Cl_2, 125.8 MHz).

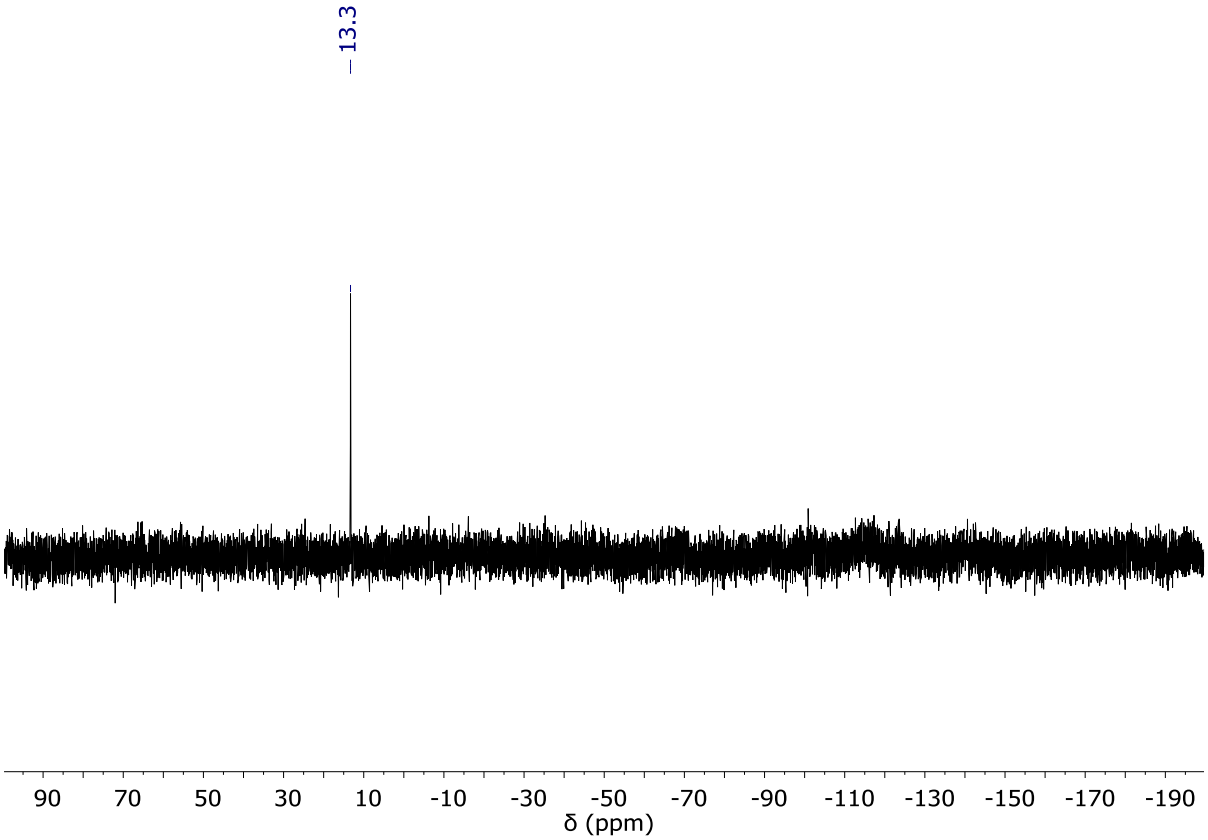

Figure S19. $^{29}Si\{^{1}H\}$ NMR spectrum of $Cl_3Si–Me_2Ge–SiCl_3$ (CD_2Cl_2, 99.4 MHz).

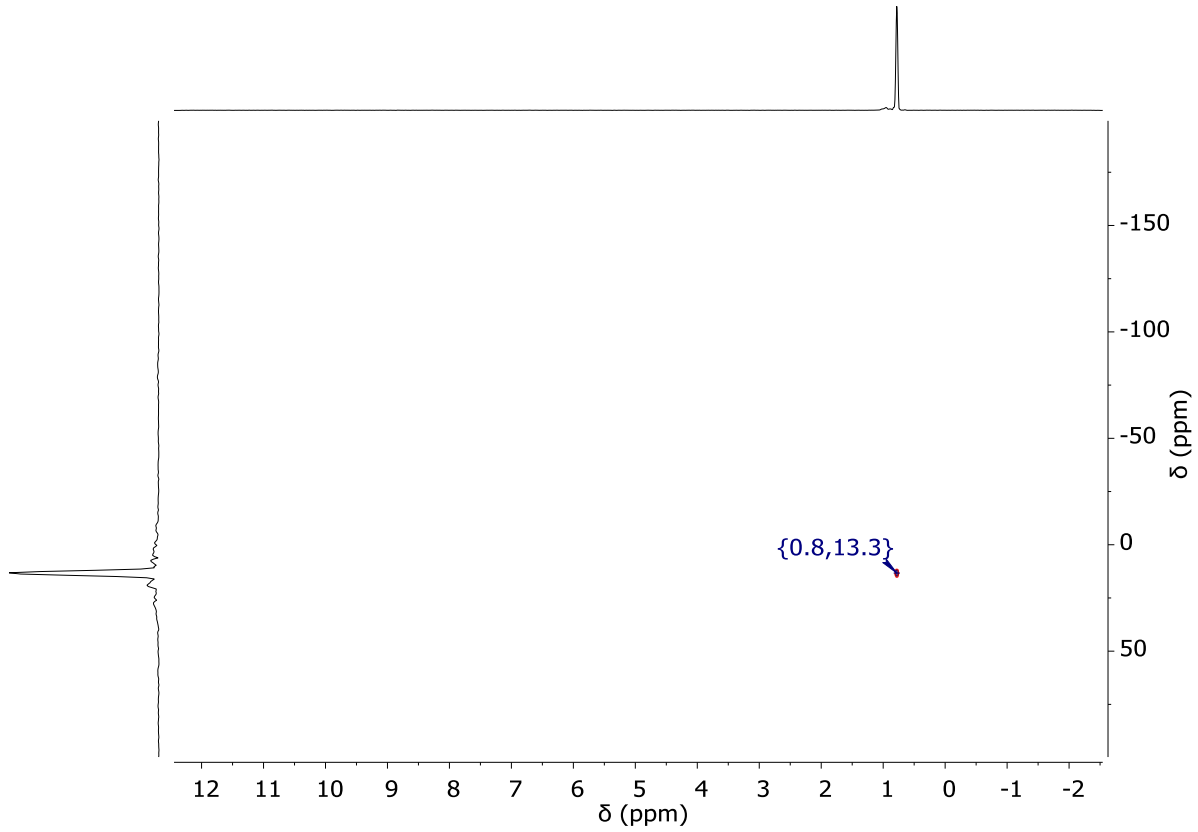

Figure S20. $^{29}Si/^{1}H$ HMBC NMR spectrum of $Cl_3Si–Me_2Ge–SiCl_3$.

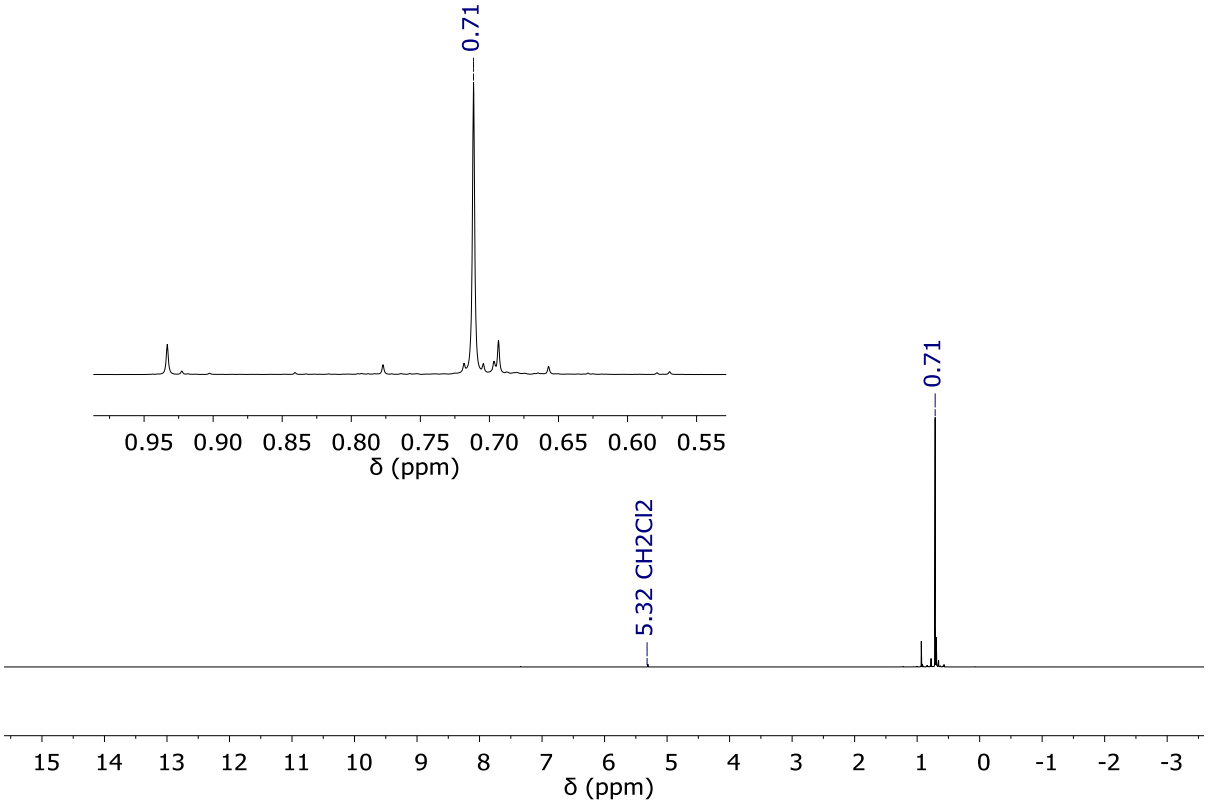

Figure S21. ^{1}H NMR spectrum of $Cl_3Si–Me_2Ge–Me_2Ge–SiCl_3$ (CD_2Cl_2, 500.2 MHz).

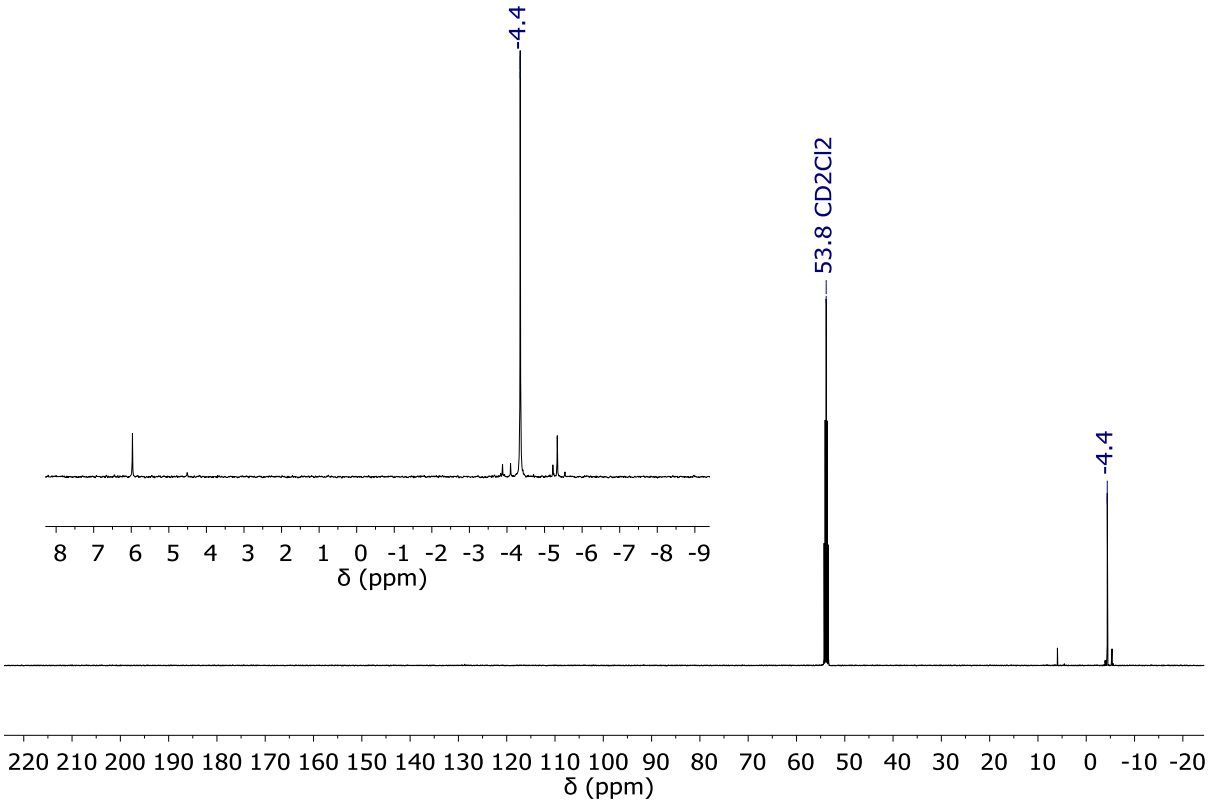

Figure S22. $^{13}C\{^{1}H\}$ NMR spectrum of $Cl_3Si–Me_2Ge–Me_2Ge–SiCl_3$ (CD_2Cl_2, 125.8 MHz).

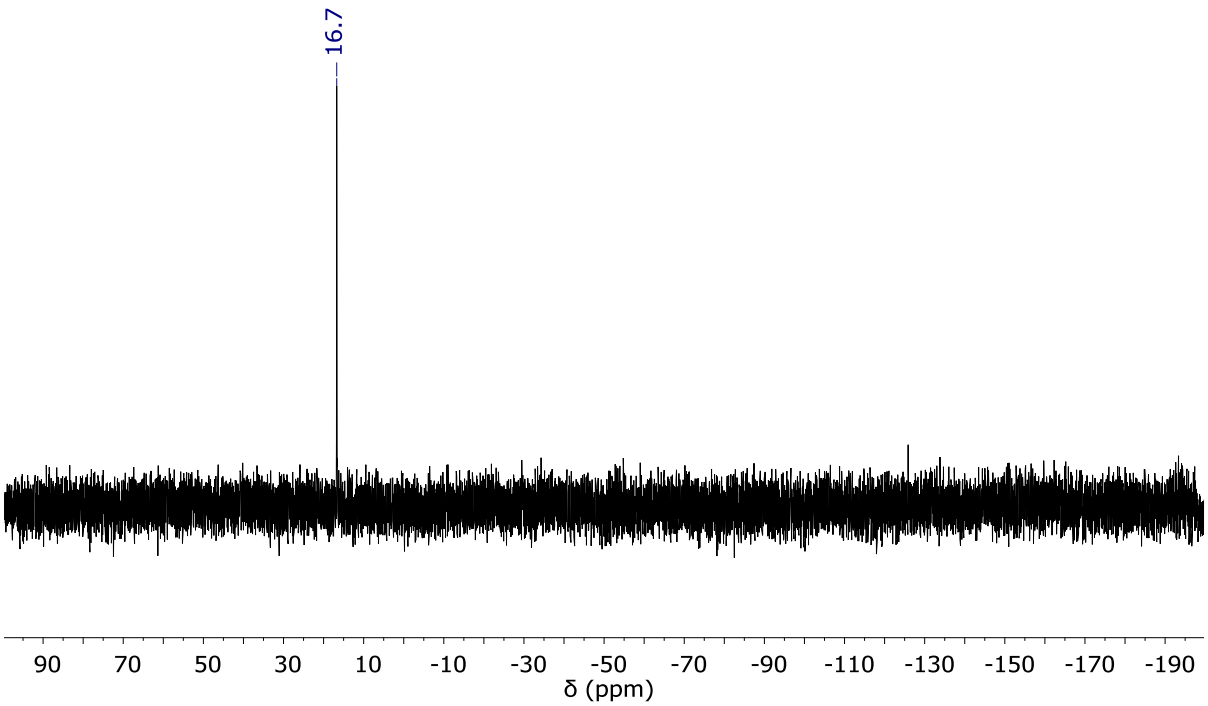

Figure S23. $^{29}Si\{^{1}H\}$ NMR spectrum of $Cl_3Si–Me_2Ge–Me_2Ge–SiCl_3$ (CD_2Cl_2, 99.4 MHz).

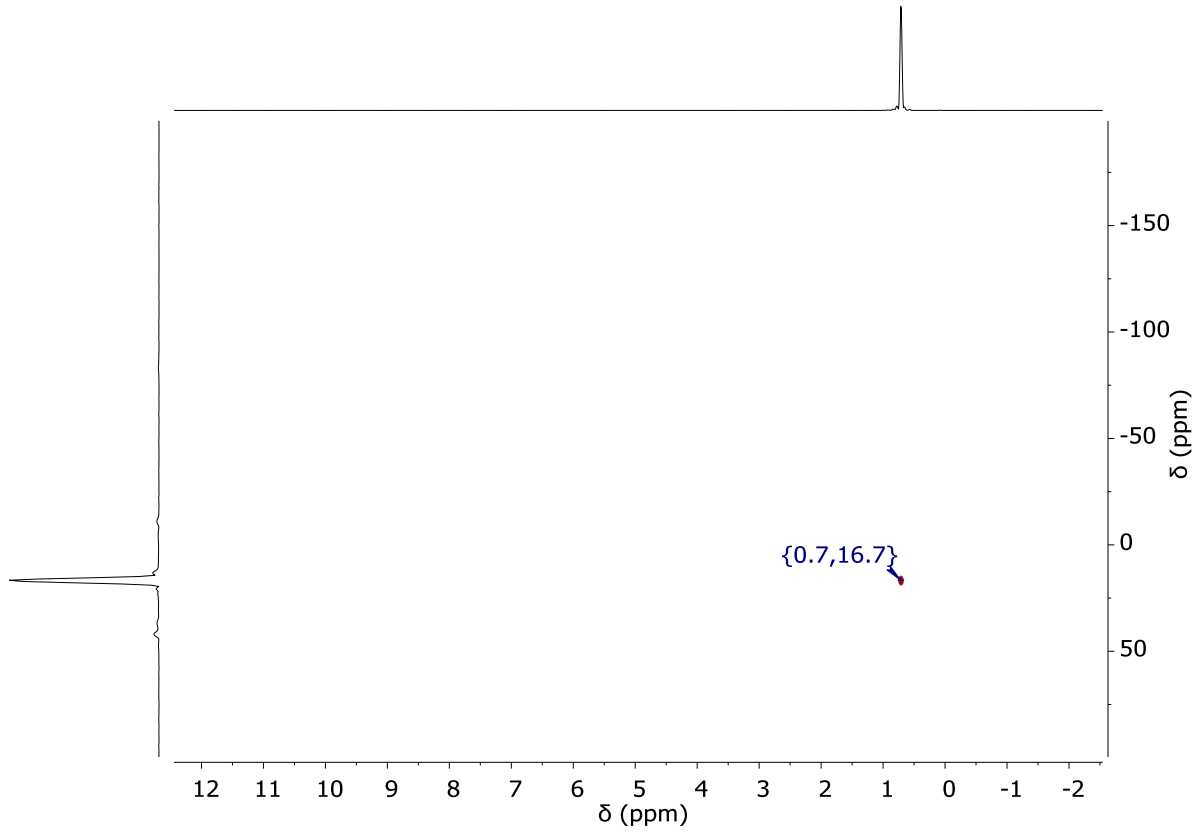

Figure S24. $^{29}Si/^{1}H$ HMBC NMR spectrum of $Cl_3Si–Me_2Ge–Me_2Ge–SiCl_3$.

3. Plots of Mass Spectra

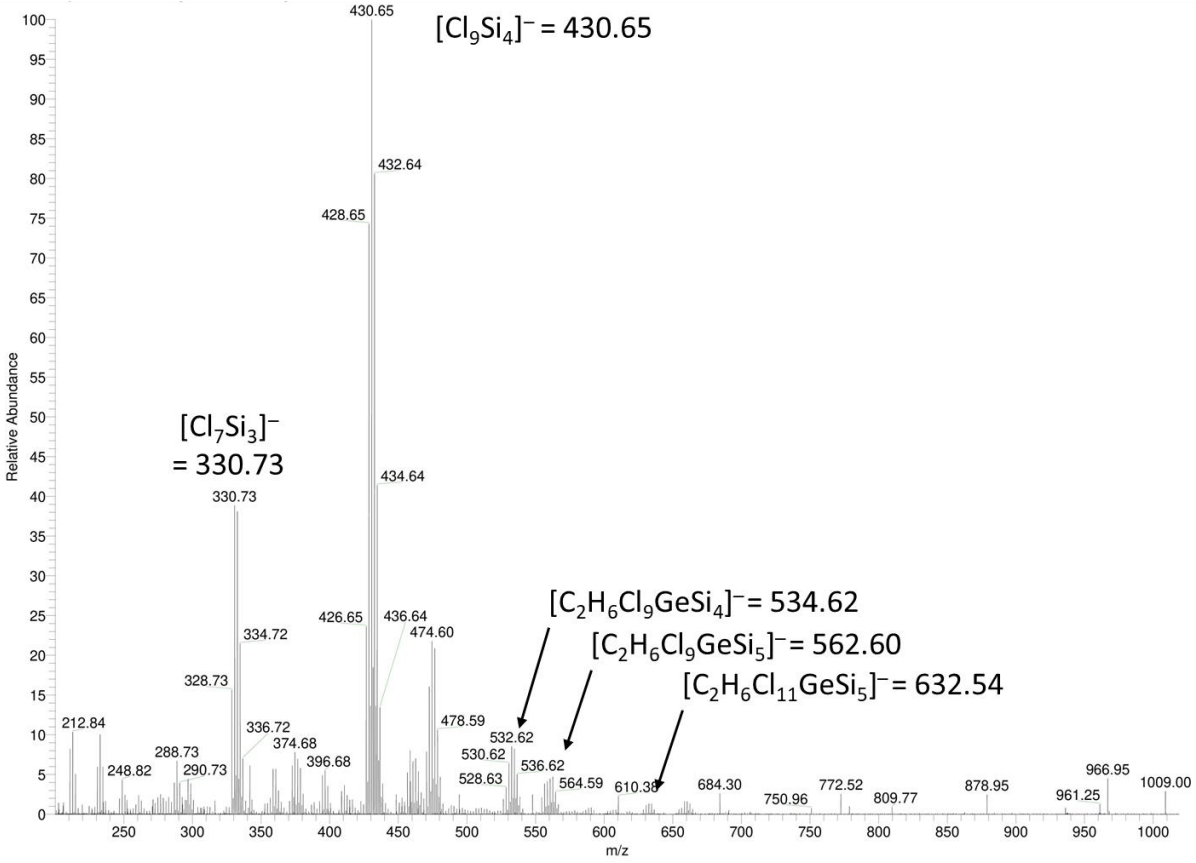

Figure S25. LDI(–) mass spectrum of [*n*Bu$_4$N]$_2$[**A**·2Cl].

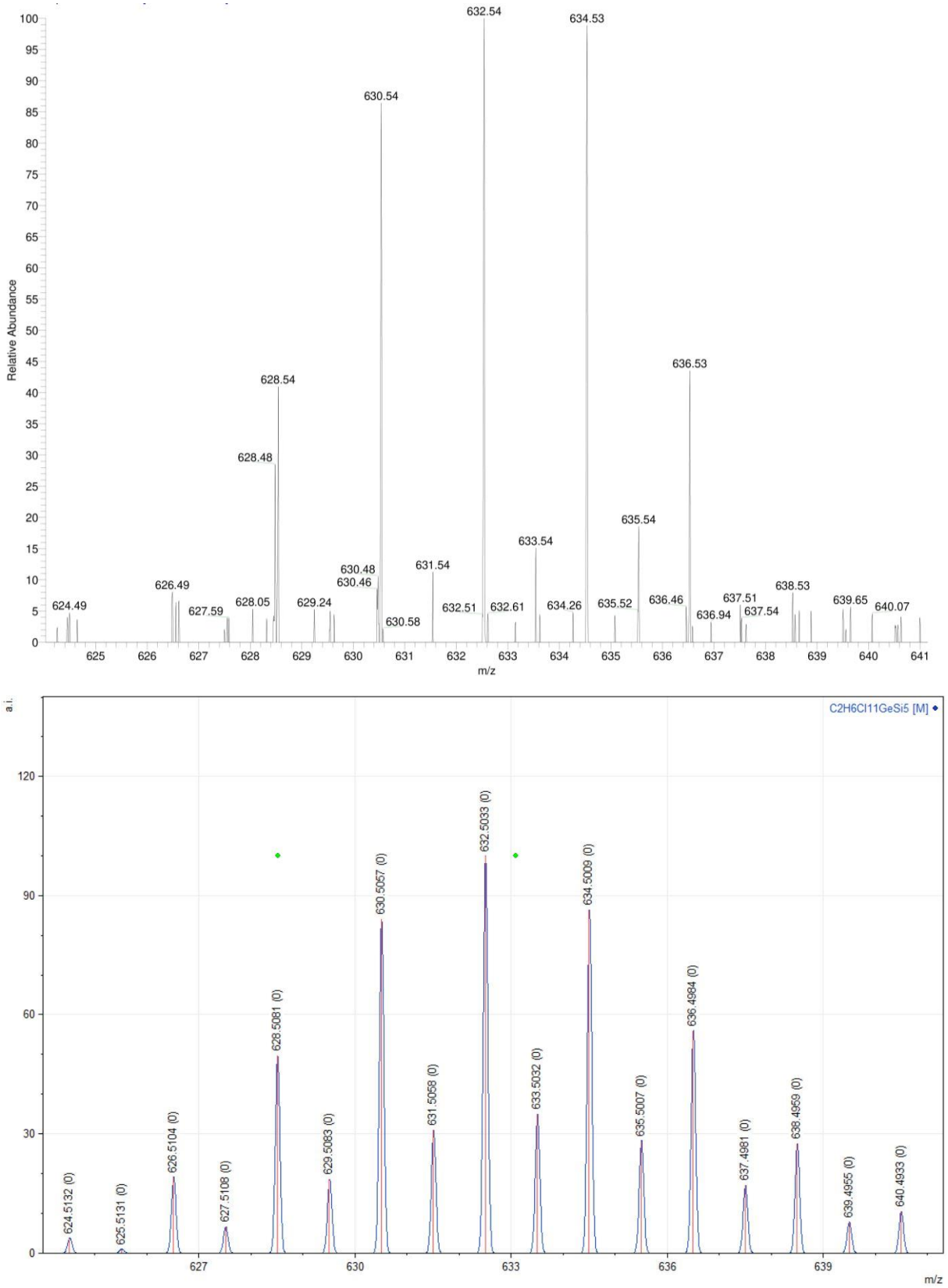

Figure S26. Measured (top, [*n*Bu$_4$N]$_2$[**A**·2Cl]) and simulated (bottom) isotopic pattern of the mono-adduct [**A**·Cl]$^-$.

4. Single-Crystal X-ray Analyses

Single-crystal diffraction data were collected at –100 °C on a *STOE IPDS II* two-circle diffractometer equipped with a *Genix 3D HS* microfocus MoK_α X-ray source (λ = 0.71073 Å). The finalizations of the data, including the empirical absorption corrections, were done using the *CrysAlisPro* software v.1.171.42.43a (Rigaku Oxford Diffraction, 2022). The structures were solved using the program *SHELXT* and refined against $|F|^2$ with full-matrix least-squares techniques using the program *SHELXL*-2018/3.[S8,S9] All H atoms were located geometrically and refined riding on the pivot atom. Some of the positions of $SiCl_2$ groups are shared with $GeMe_2$ groups with variable ratios (due to disorder). In these cases, both positions were taken into refinement assuming the same atomic coordinates and anisotropic replacement parameters (EXYZ and EADP instructions in *SHELXL-2018*). Moreover, because there is no chemical evidence for the existence of $SiMe_2$ or $GeCl_2$ groups, the same occupancy factors were assigned to Si/Cl and Ge/Me pairs.

CIF files containing the crystallographic information were deposited in the Cambridge Crystallographic Data Centre under the deposition codes CSD2217223 ([*n*Bu$_4$N]$_2$[**A**·2Cl]), 2217224 ({**A**}$_{0.917}${(SiCl$_2$)$_6$}$_{0.083}$), and 2217225 ({**B**}$_{0.95}${(SiMe$_2$)$_6$}$_{0.05}$) and can be obtained free of charge via www.ccdc.cam.ac.uk/data_request/cif. Crystallographic data and parameters of the diffraction experiments are given in Table S2.

The authors thank Dr. Matthias Meyer (Rigaku Oxford Diffraction) for his precious help with the implementation of the *CrysAlisPro* software for the *STOE IPDS II* diffraction data.

Table S2. Crystallographic data and experimental details for $[n\mathrm{Bu_4N}]_2[\mathbf{A}\cdot 2\mathrm{Cl}]$, $\{\mathbf{A}\}_{0.917}\{(\mathrm{SiCl_2})_6\}_{0.083}$, and $\{\mathbf{B}\}_{0.95}\{(\mathrm{SiMe_2})_6\}_{0.05}$.

	$[n\mathrm{Bu_4N}]_2[\mathbf{A}\cdot 2\mathrm{Cl}]$	$\{\mathbf{A}\}_{0.917}\{(\mathrm{SiCl_2})_6\}_{0.083}$	$\{\mathbf{B}\}_{0.95}\{(\mathrm{SiMe_2})_6\}_{0.05}$
Deposition code	2217223	2217224	2217225
Chemical formula	$\mathrm{C_2H_6Cl_{10}GeSi_5\cdot 2(C_{16}H_{36}N)\cdot 2(Cl)}$	$(\mathrm{C_2H_6GeSi_5Cl_{10}})_{0.917}$ $(\mathrm{Si_6Cl_{12}})_{0.083}$	$(\mathrm{C_{12}H_{36}GeSi_5})_{0.95}$ $(\mathrm{C_{12}H_{36}Si_6})_{0.05}$
M_r	1153.42	597.31	391.22
Crystal system, space group	Triclinic, $P\bar{1}$	Monoclinic, $C2/c$	Monoclinic, $C2/c$
Temperature (K)	173	173	173
a, b, c (Å)	11.2040(6), 11.7302(6), 12.2936(8)	17.6683(16), 9.7739(6), 13.5067(11)	17.9958(15), 10.1115(7), 13.9227(13)
α, β, γ (°)	90.116(5), 108.521(6), 111.813(5)	90, 109.595(10), 90	90, 108.936(10), 90
V (Å^3)	1409.03(15)	2197.4(3)	2396.3(4)
Z	1	4	4
$F(000)$	602	1159	836
D_x (Mg m^{-3})	1.359	1.806	1.084
Radiation type	Mo $K\alpha$	Mo $K\alpha$	Mo $K\alpha$
μ (mm^{-1})	1.25	2.78	1.46
Crystal shape	Prism	Prism	Plate
Color	Colorless	Colorless	Colorless
Crystal size (mm)	0.39 × 0.23 × 0.12	0.12 × 0.08 × 0.03	0.32 × 0.15 × 0.03
T_{min}, T_{max}	0.585, 1.000	0.555, 1.000	0.345, 1.000
No. of measured, independent, and observed [$I > 2s(I)$] reflections	14828, 5733, 4998	6227, 2245, 1744	6560, 2430, 2006
R_{int}	0.035	0.050	0.051
Θ values (°), max, min	26.4, 4.0	26.4, 4.1	26.4, 4.0
Range of h, k, l	h = –13→13, k = –14→14, l = –14→15	h = –22→21, k = –12→12, l = –16→16	h = –22→22, k = –12→11, l = –17→12
$R[F^2 > 2s(F^2)]$, $wR(F^2)$, S	0.033, 0.086, 1.07	0.035, 0.077, 1.03	0.033, 0.078, 1.03
No. of reflections	5733	2245	2430
No. of parameters	249	85	91
$\Delta\rho_{max}$, $\Delta\rho_{min}$ (e·Å^{-3})	0.41, –0.32	0.39, –0.33	0.31, –0.24

4.1. Single-Crystal X-ray Analysis of [*n*Bu$_4$N]$_2$[**A**·2Cl]

The ionic compound [*n*Bu$_4$N]$_2$[**A**·2Cl] crystallizes in the triclinic space group $P\bar{1}$ (No. 2). The molecule of [*n*Bu$_4$N]$_2$[**A**·2Cl] lies in the inversion center resulting in three crystallographically unique SiCl$_2$/GeMe$_2$ positions. One of them is equally shared between SiCl$_2$ and GeMe$_2$ (Si1/Ge1), while the other two are occupied purely with SiCl$_2$ (Si2 and Si3). The Si$_5$Ge ring is planar with a rms deviation from the plane of only 0.034 Å. In the crystal, two Cl$^-$ counterions are located on both sides of the E$_6$ ring (E = Si, Si/Ge) forming relatively short Cl···E intermolecular contacts of 2.9356(8) – 3.1880(6) Å (Figure S27).

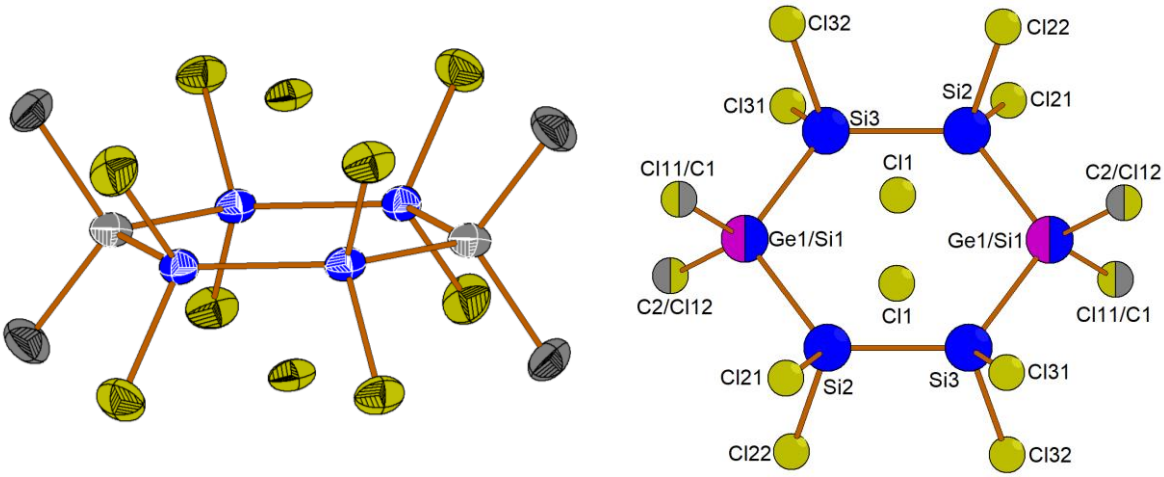

Figure S27. Molecular structure of [*n*Bu$_4$N]$_2$[**A**·2Cl] in the solid state. The cation [*n*Bu$_4$N]$^+$ is omitted for clarity. *Left:* Two vertices of the six-membered ring are equally shared between SiCl$_2$ and GeMe$_2$ (due to disorder) and are therefore shown in gray. All a.d.p. ellipsoids are shown at the 50% probability level. *Right*: The SiCl$_2$ group at Si1 is disordered with GeMe$_2$. Shown is a schematic representation of partial site occupancy factors by means of sectors. The intramolecular distance between the two coordinating Cl$^-$ ions amounts to Cl···Cl = 3.9083(9) Å.

4.2. Single-Crystal X-ray Analysis of $\{A\}_{0.917}\{(SiCl_2)_6\}_{0.083}$

The molecular compound **A** crystallizes in the monoclinic space group *C*2/*c* (No. 15) as a solid solution with $(SiCl_2)_6$, the average composition of the single crystal being $\{\mathbf{A}\}_{0.917}\{(SiCl_2)_6\}_{0.083}$. **A** is isostructural with $(SiCl_2)_6$,[S10,S11] which might explain the formation of a solid solution. The molecule lies on an inversion center (Figure S28). All three crystallographically unique $SiCl_2$ positions are shared with $GeMe_2$ on variable proportions. The unconstrained refinement of the corresponding site occupancy factors gives the chemical composition mentioned above. The Si_5Ge ring adopts a puckered chair conformation with a rms deviation from the plane of 0.68 Å.

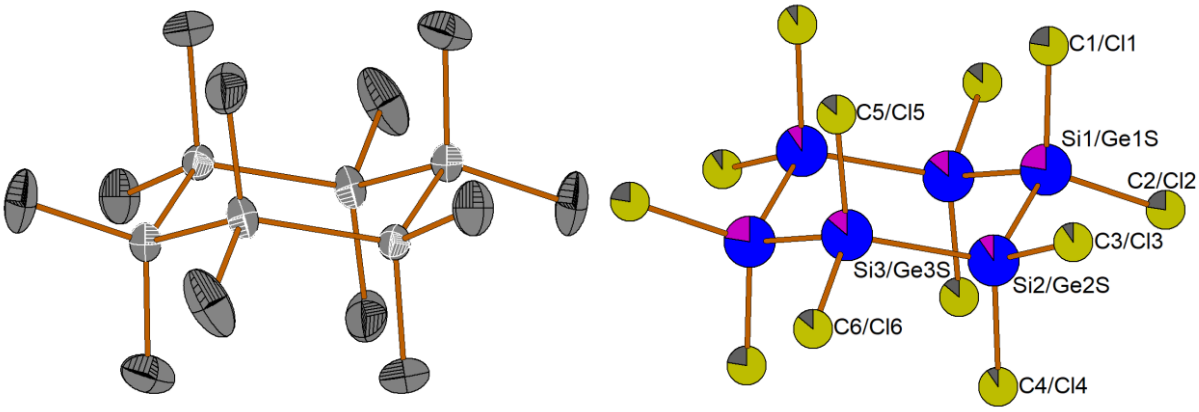

Figure S28. Molecular structure of $\{\mathbf{A}\}_{0.917}\{(SiCl_2)_6\}_{0.083}$ in the solid state. *Left:* All vertices of the six-membered ring depict positions shared between $SiCl_2$ and $GeMe_2$ (due to disorder) and are therefore shown in gray. The a.d.p. ellipsoids are shown at the 50% probability level. *Right*: Schematic representation of partial site occupancy factors by means of sectors. Only one half of the molecule is numbered for clarity.

4.3. Single-Crystal X-ray Analysis of $\{\mathbf{B}\}_{0.95}\{(SiMe_2)_6\}_{0.05}$

The molecular compound **B** crystallizes in the monoclinic space group *C*2/*c* (No. 15) as a solid solution with $(SiMe_2)_6$, the average composition of the single crystal being $\{\mathbf{B}\}_{0.95}\{(SiMe_2)_6\}_{0.05}$. **B** is isostructural with $(SiMe_2)_6$,[S11,S12] $(GeMe_2)_6$,[S13] as well as with the chlorinated compounds **A**, $(SiMeCl)_6$,[S14] $(SiMe_2)_4(SiMeCl)_2$,[S15] and $(SiCl_2)_6$.[S10,S11] **B** is located on an inversion center and all three crystallographically unique Si atoms are shared with Ge in variable proportions (due to disorder). The unconstrained refinement of the corresponding site occupancy factors points to a 'contamination' of **B** with 5% of $(SiMe_2)_6$ (note that a fitting elemental analysis was obtained). The Si_5Ge ring adopts a puckered chair conformation with a rms deviation from the plane of 0.65 Å.

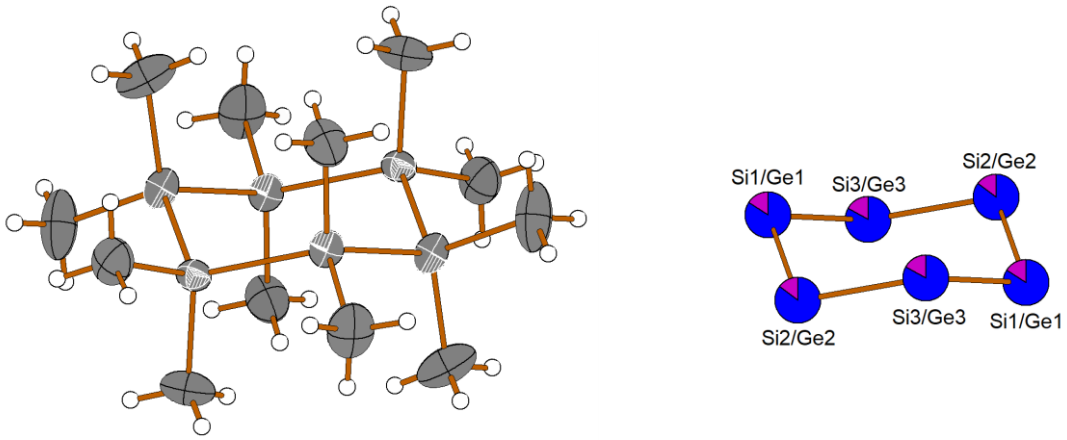

Figure S29. Molecular structure of $\{\mathbf{B}\}_{0.95}\{(SiMe_2)_6\}_{0.05}$ in the solid state. *Left:* All vertices of the six-membered ring depict positions shared between $SiMe_2$ and $GeMe_2$ (due to disorder) and are therefore shown in gray. The a.d.p. ellipsoids are shown at the 50% probability level. *Right*: Schematic representation of partial site occupancy factors by means of sectors.

5. Computational Details

In order to choose appropriate methods for optimizing the structures investigated herein, we performed geometry optimizations of $[(SiCl_2)_6 \cdot 2Cl]^{2-}$ and $[\mathbf{A} \cdot 2Cl]^{2-}$ considering three distinct DFT functionals, namely B3LYP[S16]-D3[S17](BJ)[S18], M06-2X[S19]-D3[S17], and MN15[S20]. The latter is the most recent functional from the Minnesota family which among other features has been optimized for non-covalent interactions. These calculations were performed in combination with implicit solvation by the solvent model based on density (SMD; solvent = CH_2Cl_2; ε = 8.93)[S21] and the basis set 6-31+G(d).[S22] By comparing the optimized results with the experimentally observed single-crystal X-ray structures we found averaged root mean square deviation values (RMSD; excluding H atoms) of 0.121 (B3LYP-D3(BJ)), 0.125 (M06-2X-D3), and 0.107 (MN15). Therefore, all other geometry optimizations and Hessian calculations were performed at the SMD(CH_2Cl_2)/MN15/6-31+G(d) level of theory. Optimized geometries were confirmed to be the desired minimum energy structures by vibrational frequency analysis. Single point calculations were performed at the SMD(CH_2Cl_2)/MN15/6-311++G(d,p)[S22] level to get final energy values. All enthalpy (H_{298}) and free energy (G_{298}) values were calculated for the corresponding experimental temperature at 298 K. All DFT calculations were performed using Gaussian 16, Revision B.01.[S23] Graphical representations of molecular geometries were produced with the *CYLview20* software.[S24]

5.1. Comparison of the Lewis Acidity of A, $C^{1,3}$, and $D^{1,3,5}$ with $(SiCl_2)_6$

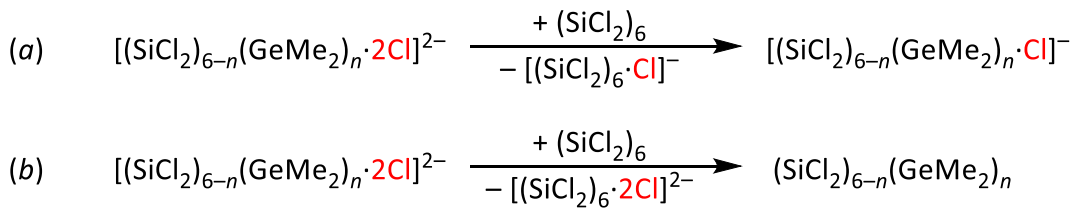

compound	*n*	$GeMe_2$-Pos.	ΔG_{298} (*a*)	ΔG_{298} (*b*)
$(SiCl_2)_6$	0	-	−3.0	0.0
A	1	1	−8.4	−14.9
$C^{1,3}$	2	1,3	−15.5	−25.8
$D^{1,3,5}$	3	1,3,5	−20.3	−36.0

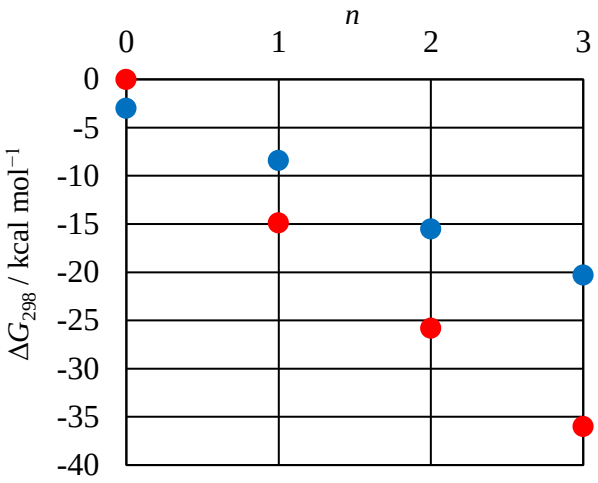

Figure S30. Top: Competition reactions between $[(SiCl_2)_{6-n}(GeMe_2)_n{\cdot}2Cl]^{2-}$ (n = 0−3) and free $(SiCl_2)_6$, where one (*a*) or two (*b*) of the complexing Cl^- ions were transferred. Bottom: Computed thermodynamics (ΔG_{298} in kcal mol^{-1}) and graphic visualization thereof (*a*: blue; *b*: red).

The transfer of one or two Cl^- ions is exothermic in all cases, indicating that $(SiCl_2)_6$ is the stronger Lewis acid compared to $(SiCl_2)_{6-n}(GeMe_2)_n$ (n = 1−3). Since the abstraction becomes gradually more exothermic with increasing $GeMe_2$ incorporation, it can be concluded that the Cl^- complexation energy of the free cyclohexatetrelanes decreases accordingly.

5.2. Comparison of the Lewis Acidity of $(SiCl_2)_6$, A, $C^{1,3}$, and $D^{1,3,5}$ with Si_2Cl_6

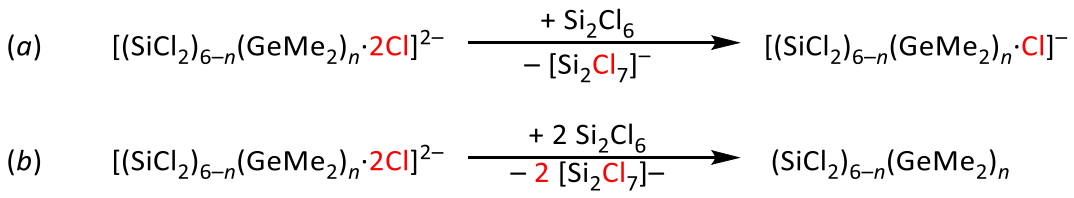

compound	*n*	$GeMe_2$-Pos.	ΔG_{298} (*a*)	ΔG_{298} (*b*)
$(SiCl_2)_6$	0	-	19.1	41.3
A	1	1	13.8	26.4
$C^{1,3}$	2	1,3	6.6	15.5
$D^{1,3,5}$	3	1,3,5	1.8	5.3

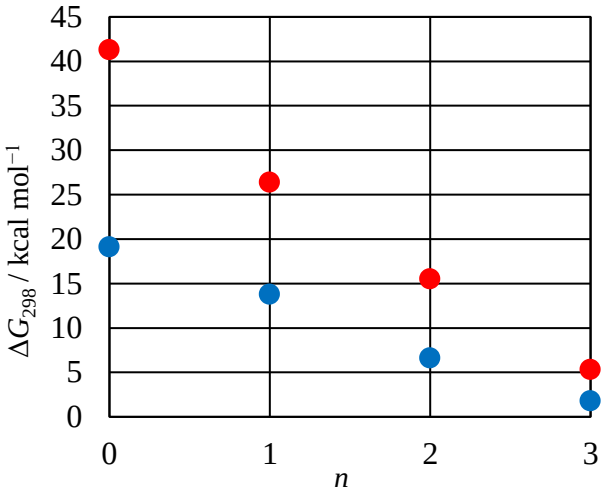

Figure S31. Top: Competition reactions between $[(SiCl_2)_{6-n}(GeMe_2)_n{\cdot}2Cl]^{2-}$ (n = 0–3) and one (*a*) or two (*b*) equivalents of Si_2Cl_6, where one or two of the complexing Cl^- ions were abstracted, respectively. Bottom: Computed thermodynamics (ΔG_{298} in kcal mol^{-1}) and graphic visualization thereof (*a*: blue; *b*: red).

Si_2Cl_6 exhibits a consistently lower Lewis acidity than the calculated cyclohexatetrelanes $(SiCl_2)_{6-n}(GeMe_2)_n$ (n = 0–3), which becomes evident from the endothermic reaction energies. However, the absolute energy difference resulting from the Cl^- transfer decreases with increasing $GeMe_2$ incorporation, which fits the general picture of decreasing Cl^- complexation energy of the free cyclohexatetrelanes.

5.3. Isodesmic Reactions to Evaluate the Relative Thermochemical Stability of the Cl^- Diadducts $[(SiCl_2)_6{\cdot}2Cl]^{2-}$, $[A{\cdot}2Cl]^{2-}$, $[C{\cdot}2Cl]^{2-}$, and $[D{\cdot}2Cl]^{2-}$

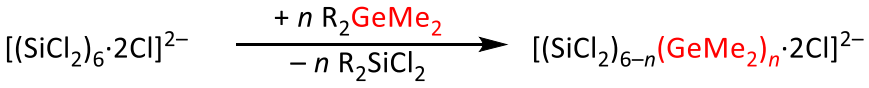

compound class	*n*	$GeMe_2$-Pos.	ΔH_{298} R = Cl	ΔH_{298} R = $SiCl_3$
$(SiCl_2)_6$	0	-	0	0
A	1	1	1.3	13.6
C	2	1,2	8.6	33.2
		1,3	4.7	29.3
		1,4	4.8	29.3
D	3	1,2,3	18.1	54.9
		1,2,4	13.5	50.3
		1,3,5	9.7	46.5

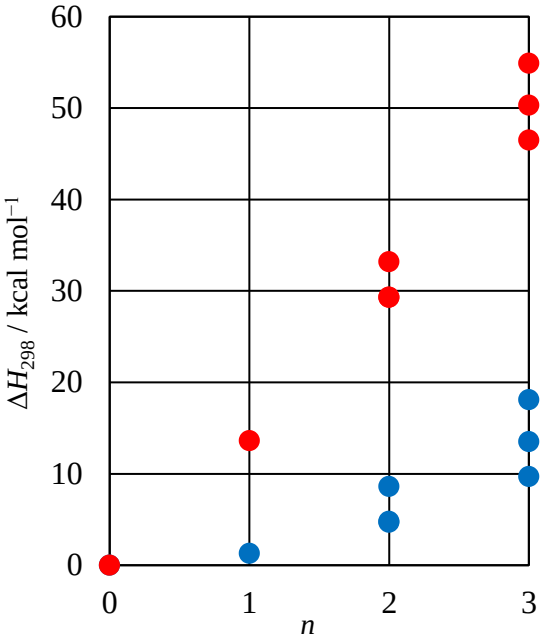

Figure S32. Top: Isodesmic reactions to evaluate the relative thermochemical stability of the Cl^- diadducts $[(SiCl_2)_{6-n}(GeMe_2)_n{\cdot}2Cl]^2$ (n = 0–3): *n* $SiCl_2$ groups in $[(SiCl_2)_6{\cdot}2Cl]^{2-}$ are replaced by *n* $GeMe_2$ moieties. R = Cl or $SiCl_3$. Bottom: Computed thermodynamics (ΔH_{298} in kcal mol^{-1}) and graphic visualization thereof (R = Cl: blue; R = $SiCl_3$: red).

The enthalpies calculated for the isodesmic reactions indicate that with increasing substitution of $SiCl_2$ by $GeMe_2$, the relative thermochemical stability decreases. This is in good agreement with the observed trends for Cl^- complexation energies of the corresponding neutral rings (cf. Figures S30 and S31). Two different substituents R were chosen to realize the formally exchanged silylenes/germylenes (R_2GeMe_2/R_2SiCl_2; R = Cl or $SiCl_3$) within the isodesmic reactions. This leads to a change in the absolute enthalpies, but the overall trend is maintained. Furthermore, it can be observed that isomers with one (or two) Ge–Ge bonds are generally higher in energy than their Si–Ge alternating counterparts (cf. $\mathbf{D^{1,2,3}}$ vs. $\mathbf{D^{1,3,5}}$).

5.4. Enthalpy and Free Energy Values of Computed Compounds

$[(SiCl_2)_6 \cdot 2Cl]^{2-}$

H_{298} = −8179.31648620 Hartree

G_{298} = −8179.41478020 Hartree

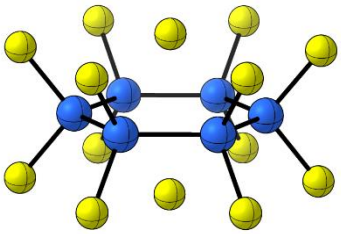

$[\mathbf{A} \cdot 2Cl]^{2-}$

H_{298} = −9126.57628383 Hartree

G_{298} = −9126.67695883 Hartree

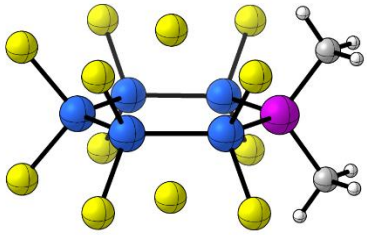

$[\mathbf{C}^{1,2} \cdot 2Cl]^{2-}$

H_{298} = −10073.82656880 Hartree

G_{298} = −10073.92951480 Hartree

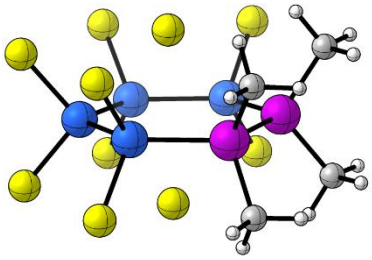

$[\mathbf{C}^{1,3} \cdot 2Cl]^{2-}$

H_{298} = −10073.83277820 Hartree

G_{298} = −10073.93599020 Hartree

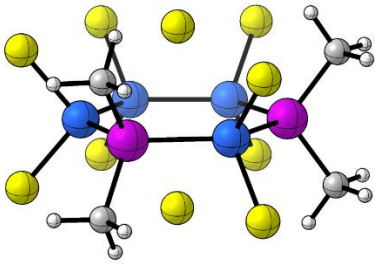

$[\mathbf{C}^{1,4} \cdot 2Cl]^{2-}$

H_{298} = −10073.83275000 Hartree

G_{298} = −10073.93616400 Hartree

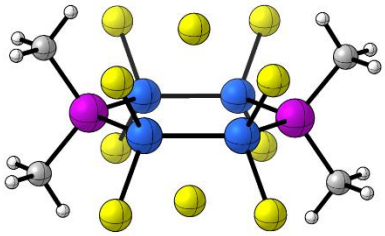

$[\mathbf{D}^{1,2,3} \cdot 2Cl]^{2-}$

H_{298} = −11021.07343320 Hartree

G_{298} = −11021.17968920 Hartree

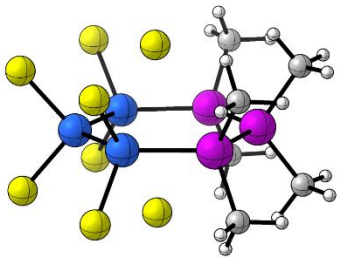

$[\mathbf{D}^{1,2,4}\cdot 2Cl]^{2-}$

$\boldsymbol{H}_{298}$ = −11021.08072870 Hartree

$\boldsymbol{G}_{298}$ = −11021.18697770 Hartree

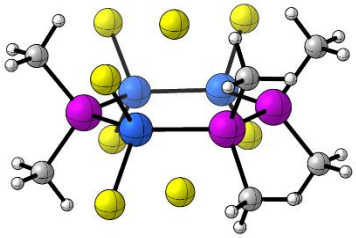

$[\mathbf{D}^{1,3,5}\cdot 2Cl]^{2-}$

$\boldsymbol{H}_{298}$ = −11021.08687120 Hartree

$\boldsymbol{G}_{298}$ = −11021.19680220 Hartree

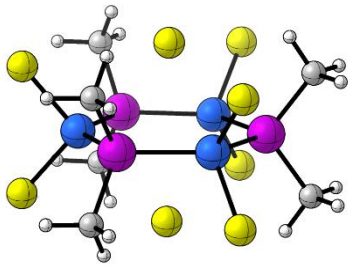

$[(SiCl_2)_6\cdot Cl]^{-}$

$\boldsymbol{H}_{298}$ = −7718.96755492 Hartree

$\boldsymbol{G}_{298}$ = −7719.06455592 Hartree

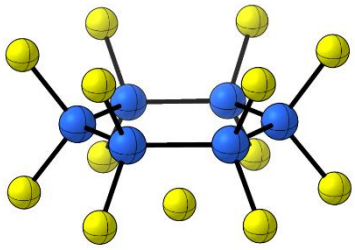

$[\mathbf{A}\cdot Cl]^{-}$

$\boldsymbol{H}_{298}$ = −8666.23881281 Hartree

$\boldsymbol{G}_{298}$ = −8666.33530381 Hartree

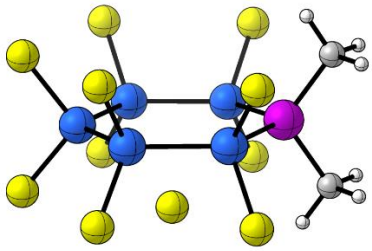

$[\mathbf{C}^{1,3}\cdot Cl]^{-}$

$\boldsymbol{H}_{298}$ = −9613.50632764 Hartree

$\boldsymbol{G}_{298}$ = −9613.60569364 Hartree

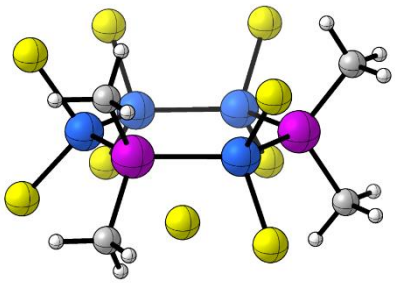

$[\mathbf{D}^{1,3,5}\cdot Cl]^{-}$

$\boldsymbol{H}_{298}$ = −10560.76981820 Hartree

$\boldsymbol{G}_{298}$ = −10560.87413620 Hartree

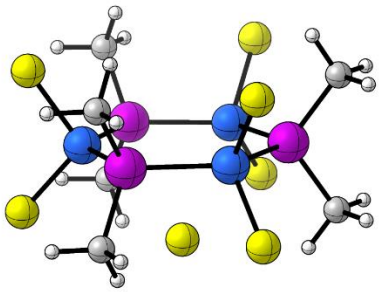

$(SiCl_2)_6$

***H*$_{298}$ =** −7258.61547881 Hartree

***G*$_{298}$ =** −7258.70954381 Hartree

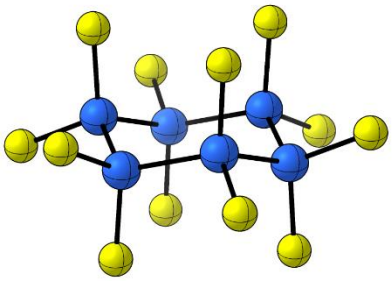

A

***H*$_{298}$ =** −8205.89746397 Hartree

***G*$_{298}$ =** −8205.99551197 Hartree

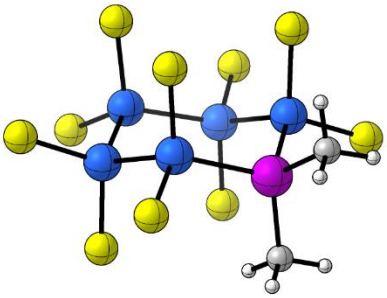

C^{1,3}

***H*$_{298}$ =** −9153.17318946 Hartree

***G*$_{298}$ =** −9153.27189546 Hartree

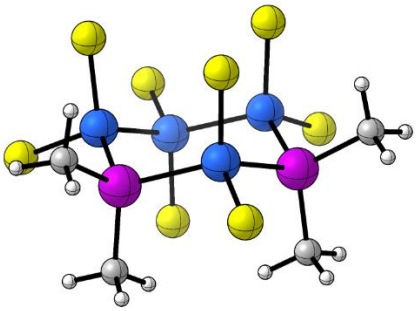

D^{1,3,5}

***H*$_{298}$ =** −10100.44360790 Hartree

***G*$_{298}$ =** −10100.54887190 Hartree

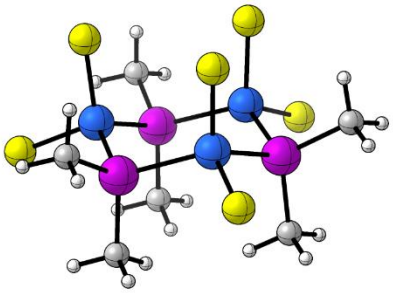

Si_3Cl_8

***H*$_{298}$ =** −4549.66075704 Hartree

***G*$_{298}$ =** −4549.72986804 Hartree

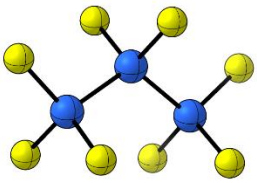

$Cl_3Si{-}Me_2Ge{-}SiCl_3$

***H*$_{298}$ =** −5496.94223083 Hartree

***G*$_{298}$ =** −5497.01295483 Hartree

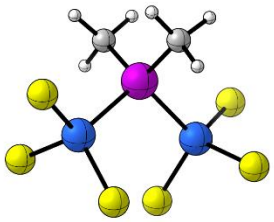

$SiCl_4$

***H*$_{298}$ =** −2130.12045342 Hartree

***G*$_{298}$ =** −2130.16041042 Hartree

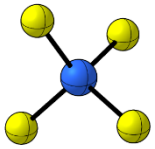

Me_2GeCl_2

***H*$_{298}$ =** −3077.42520504 Hartree

***G*$_{298}$ =** −3077.38238204 Hartree

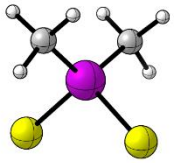

Si_2Cl_6

***H*$_{298}$ =** −3339.89047952 Hartree

***G*$_{298}$ =** −3339.94446652 Hartree

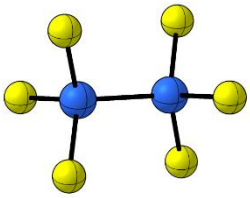

$[Si_2Cl_7]^-$

***H*$_{298}$ =** −3800.20670061 Hartree

***G*$_{298}$ =** −3800.26418961 Hartree

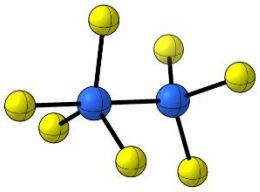

6. References

S1 G. R. Fulmer, A. J. M. Miller, N. H. Sherden, H. E. Gottlieb, A. Nudelman, B. M. Stoltz, J. E. Bercaw and K. I. Goldberg, *Organometallics*, 2010, **29**, 2176–2179.

S2 M. Strohalm, D. Kavan, P. Novák, M. Volný and V. Havlíček, *Anal. Chem.*, 2010, **82**, 4648–4651.

S3 C. Kunkel, M. Bolte, H. Lerner, P. Albert and M. Wagner, *Chem. Commun.*, 2021, **57**, 12028–12031.

S4 E. Carberry and B. D. Dombek, *J. Organomet. Chem.*, 1970, **22**, c43–c47.

S5 L. Müller, W.-W. du Mont, F. Ruthe, P. G. Jones and H. C. Marsmann, *J. Organomet. Chem.*, 1999, **579**, 156–163.

S6 B. Köstler, M. Bolte, H.-W. Lerner and M. Wagner, *Chem. – A Eur. J.*, 2021, **27**, 14401–14404.

S7 J. Tillmann, L. Meyer, J. I. Schweizer, M. Bolte, H. W. Lerner, M. Wagner and M. C. Holthausen, *Chem. - A Eur. J.*, 2014, **20**, 9234–9239.

S8 G. M. Sheldrick, *Acta Crystallogr. Sect. A.*, 2015, **71**, 3–8.

S9 G. M. Sheldrick, *Acta Crystallogr, Sect. C.*, 2015, **71**, 3–8.

S10 X. Dai, S.-B. Choi, Ch. W. Braun, P. Vaidya, S. Kilina, A. Ugrinov, D. L. Schulz and P. Boudjouk, *Inorg. Chem.*, 2011, **50**, 4047–4053.

S11 Y. Omatsu, Y. Mizuhata and N. Tokitoh, *Z. Anorg. Allgem. Chem.*, 2018, **644**, 930–934.

S12 H. L. Carrell and J. Donohue, *Acta Crystallogr. Sect. B.*, 1972, **28**, 1566–1571.

S13 M. Holbling, M. Flock, J. Baumgartner and K. Hassler, *Eur. J. Inorg. Chem.*, 2007, **31**, 4952–4957.

S14 S. J. Park, H. M. Cho, M. E. Lee, M. Kim, K. Han, S. Hong, S. Lim, H. Lee, B. Hwang, S. K. Kim, S. Shim, P. Kang and M.-G. Choi, *J. Mater. Chem. C*, 2015, **3**, 239–242.

S15 D. Yu. Larkin, A. A. Korlyukov, E. V. Matukhina, M. I. Buzin, N. A. Zhernyavskaya, M. Yu. Antipin and A. I. Chernyavsky. *Russ. Chem. Bull.*, 2005, **54**, 1612–1622.

S16 a) S. H. Vosko, L. Wilk and M. Nusair, *Can. J. Phys.*, 1980, **58**, 1200–1211; b) C. Lee, W. Yang and R. G. Parr, *Phys. Rev. B*, 1988, **37**, 785–789; c) A. D. Becke, *J. Chem. Phys.*, 1993, **98**, 5648–5652; d) P. J. Stephens, F. J. Devlin, C. F. Chabalowski and M. J. Frisch, *J. Phys. Chem.*, 1994, **98**, 11623–11627.

S17 S. Grimme, J. Antony, S. Ehrlich and H. Krieg, *J. Chem. Phys.*, 2010, **132**, 154104.

S18 S. Grimme, S. Ehrlich and L. Goerigk, *J. Comput. Chem.*, 2011, **32**, 1456–1465.

S19 Y. Zhao and D. G. Truhlar, *Theor. Chem. Acc.*, 2008, **120**, 215–241.

S20 H. S. Yu, X. He, S. L. Li and D. G. Truhlar, *Chem. Sci.*, 2016, **7**, 5032–5051.

S21 A. V. Marenich, C. J. Cramer and D. G. Truhlar, *J. Phys. Chem. B*, 2009, **113**, 6378–6396.

S22 a) R. Ditchfield, W. J. Hehre and J. A. Pople, *J. Chem. Phys.*, 1971, **54**, 724–728; b) W. J. Hehre, R. Ditchfield and J. A. Pople, *J. Chem. Phys.*, 1972, **56**, 2257–2261; c) P. C. Hariharan and J. A. Pople, *Theoret. Chim. Acta*, 1973, **28**, 213–222; d) J. D. Dill and J. A. Pople, *J. Chem. Phys.*, 1975, **62**, 2921–2923; e) T. Clark, J. Chandrasekhar, G. W. Spitznagel and P. V. R. Schleyer, *J. Comput. Chem.*, 1983, **4**, 294–301.

S23 M. J. Frisch, G. W. Trucks, H. B. Schlegel, G. E. Scuseria, M. A. Robb, J. R. Cheeseman, G. Scalmani, V. Barone, B. Mennucci, G. A. Petersson, H. Nakatsuji, M. Caricato, X.

Li, H. P. Hratchian, A. F. Izmaylov, J. Bloino, G. Zheng, J. L. Sonnenberg, M. Hada, M. Ehara, K. Toyota, R. Fukuda, J. Hasegawa, M. Ishida, T. Nakajima, Y. Honda, O. Kitao, H. Nakai, T. Vreven, J. A. Montgomery Jr., J. E. Peralta, F. Ogliaro, M. Bearpark, J. J. Heyd, E. Brothers, K. N. Kudin, V. N. Staroverov, R. Kobayashi, J. Normand, K. Raghavachari, A. Rendell, J. C. Burant, S. S. Iyengar, J. Tomasi, M. Cossi, N. Rega, J. M. Millam, M. Klene, J. E. Knox, J. B. Cross, V. Bakken, C. Adamo, J. Jaramillo, R. Gomperts, R. E. Stratmann, O. Yazyev, A. J. Austin, R. Cammi, C. Pomelli, J. W. Ochterski, R. L. Martin, K. Morokuma, V. G. Zakrzewski, G. A. Voth, P. Salvador, J. J. Dannenberg, S. Dapprich, A. D. Daniels, Ö. Farkas, J. B. Foresman, J. V Ortiz, J. Cioslowski and D. J. Fox, *Gaussian 16, Revision B.01*, Gaussian, Inc., Wallingford CT, 2016**.**

S24 C. Y. Legault, *CYLview20*, Université de Sherbrooke, 2020 (http://www.cylview.org).